Active Control of Supersonic Impingement Tones using Microjets

by

Jae Jeen Choi

Submitted to the Department of Mechanical Engineering
in partial fulfillment of the requirements for the degree of

Master of Science in Mechanical Engineering

at the

MASSACHUSETTS INSTITUTE OF TECHNOLOGY

September 2003

Author .....
Department of Mechanical Engineering
August 8, 2003

Certified by .....
Anuradha M. Annaswamy
Senior Research Scientist
Thesis Supervisor

Accepted by .....
Ain A. Sonin
Chairman, Department Committee on Graduate Students

Active Control of Supersonic Impingement Tones using Microjets

by

Jae Jeen Choi

Submitted to the Department of Mechanical Engineering
on August 8, 2003, in partial fulfillment of the
requirements for the degree of
Master of Science in Mechanical Engineering

Abstract

High speed jet impinging on an obstacle generates distinct noise. If the jet flow exits with supersonic speed, the noise becomes more profound and causes many detrimental effects to the environment. STOVL exposed such tones experiences many adverse effects such as lift loss, sonic fatigue on the aircraft structure and ground erosion. Until now the impinging tone along with several adverse effects are thought to be originated by the feedback mechanism due to the presence of wall near the nozzle exit. As the acoustic waves reach the nozzle lip they excite the instability traveling downstream in the jet shear layer. These instability waves rapidly develop into large-scale coherent shear layer structures while traveling downstream. On impinging on the ground plane, this structure generates high amplitude pressure fluctuation, which generates acoustic wave, thus completing feedback loop. Hence, the noise reduction trial should be conducted to disrupt the feedback loop.

Many researchers have tried to destroy the feedback loop using passive and active way, but the reduction was confined only on specific operating conditions or so small extent compared to no control case. Recently, an attempt [1] using microjet showed a promising result. Because it is micro-scaled valve created by MEMS technology, microjet can be placed on any location without any space limitation and optimal flow control is possible by activating the supersonic microjet to desired command. In addition, since the microjet just affects the target properties without interfering other physical condition, it was accepted as the desired actuator. In this thesis, a special control strategy based on POD mode showed better reduction throughout several operating conditions. It is a kind of a parametric control strategy which sets the microjet pressure proportional to the shape of the most energetic mode. The reasoning for this control is based on the fact that the supersonic microjets attached near the nozzle exit may disrupt the feedback loop partially intercepting the upstream propagating acoustic disturbance or distort the coherent shear layer instabilities consequently disrupting their interaction with the acoustic field.

So far, the analysis based on a model has not been tried in depth. The second contribution of this thesis is the development of a reduced-order model. In this literature,

an updated form of Tam's [40] describing impinging jet on a wall, is suggested and its validity is supported from several experimental data conducted in Florida State University. Furthermore, the mechanism of noise reduction and the effectiveness of the POD based closed-loop control strategy is introduced. Finally, a closed-loop control strategy expecting uniform reduction regardless of the ground effect over the entire range and varying operating conditions is experimentally tested and implemented in a STOVL facility at Mach 1.5.

Thesis Supervisor: Anuradha M. Annaswamy
Title: Senior Research Scientist

Acknowledgments

First of all, I would like to thank Professor Anuradha M. Annaswamy for her nice guidance for the past 2 years. During those days, her advice gave me good intuition and a way of thinking needed for solving many engineering problems. I owed a lot of things to my research group members. I think the group is ideal combination in that each one has great talent that the others do not have. Prof. Ghoniem, a great scholar in Fluid mechanics area, brought confidence in making the impingement tone model. Dae Hyun Wee is mathematically well trained, Sung Bae Park has great intuition on solving engineering problems. I thank all of them for keeping an eye on my research and giving a constant feedback. I also owe a great deal to my colleague Sahoo not only for research work but for improving my language skill. Whenever I confronted a problem, discussions with him always give me a breakthrough.

I appreciate to Florida State University members too much, especially Prof. Krothapalli, Prof. Farrukh Alvi and his students, Okechukwu Egungwu, Huadong Lou. Because they are the experimental experts, we can do our research more efficiently. Without their efforts, I couldn't complete the experiment yet. Working with them was great pleasure to me.

I specially thank to my parents. Byung Tae Choi and Jung Mi Park. They initiated my dream studying in MIT and encouraged me to make it come true. Finally, I appreciate to my brother, Jae Woong Choi, for helping me to be mentally strong during life in U.S.

This work was supported by a grant from the Airforce Office of Scientific Research, through the Unsteady Aerodynamics and Hypersonic program.

Contents

1 Introduction **10**

2 Reduced Order Model of Impingement Tone **15**

2.1 Physical Model and Its State-Space Form 16

2.1.1 Vortex Sheet Model 16

2.1.2 A Control-Oriented Model 25

2.1.3 Model Validation 26

2.1.4 State-Space Equations 28

2.2 Proper Orthogonal Decomposition 30

2.2.1 The Karhunen-Loeve Expansion 31

2.2.2 Optimality of the Karhunen-Loeve Expansion 32

2.2.3 Method of Snapshots 35

3 POD-based Closed-loop Control Strategy **39**

3.1 The POD method in flow field 40

3.2 The Control Strategy 41

3.3 The Experimental Support 44

3.3.1 The Experimental Setup 44

3.3.2 The Previous Study 48

3.3.3 Result and Possible Mechanism of Microjet Effect 50

4 Summary and Concluding Remark **54**

A Tables **56**

B Figures 58

List of Figures

B-1 Flow field created by the propulsion system around a STOVL aircraft 59

B-2 Instantaneous shadowgraphs of a supersonic impinging jet at NPR = 3.7, $h/d = 5.5$ 59

B-3 The experimental set up of Fluid Mechanics Research Laboratory in Florida State University 60

B-4 Schematic of the experimental arrangement 60

B-5 Schematic of the lift plate 61

B-6 Vortex-sheet model for impingement tones control problem 61

B-7 Expected shear layer intensity distribution (a), coordinate system used for calculating acoustic excitation (b). 62

B-8 Schematic diagram of PIV mearsuring process 62

B-9 Instantaneous shadowgraph images of a supersonic impinging jets without (a) and with control (b) at NPR = 3.7, $h/d = 4$ 63

B-10 Reductions in fluctuating pressure intensities as a function of h/d, NPR = 5 (a) and NPR = 3.7 (b) 63

B-11 PLS images taken at one diameter downstream of nozzle, NPR = 5.0, $h/d = 4.0$; (a)Instantaneous image, (b)Time-averaged image 64

B-12 Streamwise vorticity distribution at the z/d = 1.0 cross plane of the jet flow NPR = 5.0, $h/d = 4.0$; (a)Instantaneous image, (b)Time-averaged image 65

B-13 Frequency spectra for unsteady pressure on the lift plate of NPR = 3.7, $h/d = 4.0$ 66

B-14 Microjet effectiveness on different trials (NPR = 3.7) conducted on Sep. 2000 (a) and Dec. 2001 (b) 66
B-15 Frequency spectra for unsteady pressure on the lift plate of NPR = 3.7, h/d = 6.0 (a) and model prediction of NPR = 6.0 (b) 67
B-16 The idealized centerline velocity 68
B-17 Frequency spectra of the unsteady pressure on the lift plate at NPR = 3.7: (a) Experimental data, and (b) Model prediction. Note that the amplitude scales in (a) and (b) are different. 69
B-18 Variation of frequency of three impinging tones with h/d at NPR = 3.7: (a) Experimental data, and (b) Model Prediction. 70
B-19 Peak frequency interval of experimental data and model prediction (NPR=3.7, M = 1.5) 71
B-20 The first mode shape and suggested pressure for each height. x axis is transducer position, y axis is normalized mode value 72
B-21 Overall sound pressure levels(OASPL) for different control (NPR=3.7) 73

List of Tables

A.1 The energy content of the first four modes at each height (NPR=3.7) 56

A.2 Comparison of peak frequency interval (Hz) NPR=3.7, M =1.5 . . . 57

Chapter 1

Introduction

High-speed jet issuing from the nozzle often generates the acoustic field dominated by discrete, high-amplitude tones. For example, screech tones are present in non-ideally expanded jet, edge tones are dominant in the presence of edge shaped body and impingement tones are conspicuous when a supersonic jet impinges on a surface. Those tones are undesirable for any kind of mechanical system in itself because they cause a very detrimental effect such as sonic fatigue on the body facing the noise source. Especially, the impingement tone is unfavorable in designing efficient Short Take-off and Vertical Landing(STOVL) aircraft. Besides the purely acoustic damage, the flow field induced by the resonance brings very severe adverse effects on the ground and the aircraft itself too as described in Fig. B-1. The flow field causes the ambient flow to entrain into the gap between the aircraft and the ground that a large amount of lift loss are generated. The engine inlet suffers from hot gas ingestion and the ground erosion happens from impinging hot flow. These phenomena are thought to be more serious in the JSF(Joint Strike Fighter), a new version of STOVL aircraft, because the operating condition is supersonic [29] region. The understanding of the impinging jet flow is definitely necessary in designing the STOVL aircraft.

Hence, many researchers have tried to find the origin of noise sources and suppress them using various ways so far. Regardless of the specific nature of the tones, a host of studies on the aeroacoustics of impinging jets by Neuwarth [24], Powell [28], Tam and Ahuja [40], and more recently Krothapalli et al. [19] have clearly established

that the self-sustained, highly unsteady behavior of the jet and the resulting impinging tones are governed by a feedback mechanism. It is well-accepted that they are governed by a feedback mechanism that strongly couples the fluid and acoustic field and this coupling occurs in the jet shear layer near the nozzle exit, a region of receptivity. These feedback interactions occur thus: Instability waves are generated by the acoustic excitation of shear layer near the nozzle exit, which then convect down and evolve into spatially coherent large-scale structures. On impinging on the ground, these structures generate high amplitude pressure perturbation, which in turn produce waves of neutral acoustic mode of the jet. As the acoustic wave reaches to the nozzle exit, it excites the shear layer again, thereby closing the feedback loop.

The presence of such large-scale structures, not normally present in such high speed jets, can be confirmed from the shadowgraph image shown in Fig. B-2. The high entrainment rates of the ambient fluid associated with such large-scale structure are thought to be largely responsible for the increased lift loss.

The logical approach to controlling the adverse ground effect is to disrupt the feedback mechanism responsible for this behavior. A number of researchers have attempted various passive and active methods in order to accomplish this goal. In the context of intercepting the feedback loop, Glass [12] and Poldervaart et al. [26] tried a passive control method by placing a plate normal to the centerline. In this way, they were able to reduced the overall noise level a certain degree. Motivated by the previous result, Elavarasan et al.[11] conducted similar experiment and have achieved about 11 dB reduction in the overall sound pressure level and recovery of about 16% lift loss. This passive control method appears to weaken the feedback loop and prevent the onset of self-sustained oscillations in the jet and result in the suppression of large-scale motion. However, the effect of such a passive approach is confined to a limited range of operating condition, especially for impinging jets. Because a small change in distance between nozzle to ground plate (h/d) leads to significant change in amplitude and frequency of impinging tone (Alvi and Iyer [2]), the control strategy for the suppression of the impinging tones should be active and adaptive for the varying operating condition. Such active approaches have also been

suggested more recently, in the literature (for example, Sheplak and Spina [32], Shih et al. [33]). In Sheplak and Spina [32]), Sheplak and Spina used a high speed co-flow to keep the main flow jet from acoustic wave. Their investigations showed a reduction of 10-15 dB in the near field broad band noise under specific core to ambient velocity ratio. To realize the effect, it was required for the co-flow flux should at least be 20% to 25% of the main jet. Shih et al. [33], upgrading the experiment, used a counter co-axial flow near the nozzle exit and were able to suppress screech tones of ideally expanded jet. However, those active control schemes required additional design modification in the nozzle part and high operating power. Consequently, such approaches are somewhat impractical for implementation in a real aircraft.

A few years ago, a study was initiated at the Fluid Mechanics Research Laboratory (FMRL) of Florida State University, in Tallahassee, Florida, with the aim of understanding and controlling supersonic impinging jet flows in order to substantially reduce the ground effect. In this study, Alvi et al. [1] and Shih et al. [35] used arrays of supersonic microjets to control supersonic impinging jets and successfully reduced lift loss by as much as 40% accompanied by a 10-11 dB reduction in the fluctuating pressure load on the lift and ground surface. They introduced microjets for noise reduction with the same motivation as the aforementioned papers trying to shield the main jet from outer acoustic perturbation but the result was more dramatic.

In Alvi et al.'s[1] paper, we can see the microjet effect on noise reduction was much greater than any other actuators so far. However, the performance using the microjet actuators was observed to depend too much on the height. It should be noted that the control strategy used was one where air-flow was introduced through the microjets at a constant 100 psi chamber pressure. This strategy is referred to as "symmetric control" in this thesis, and can be viewed as an "open-loop" control strategy which neglects changing flow conditions for different heights. Hence, to achieve a uniform performance for the different operating condition, a different control strategy that "adapts" to the changing flow conditions should be introduced. Such an active-adaptive strategy should take into consideration the changing flow conditions during taking off and hovering moment of the real STOVL aircraft.

The microjet has many advantages over previous actuators from manufacturing, designing as well as practical points of view [1]. For example, microjets can be produced in large quantities to lower the unit production cost. Because of the small size, they can be operated without any spacing limitation and consume a small amount of flow rate to cause the reduction effect. Along with other electrical devices, they can be integrated into sensor/actuator active control system. Moreover, in contrast to the traditional passive control method, each microjet can be switched on and off strategically that it will be able to avoid the degradation of performance when the control is not necessary.

In the previous paper [35], the fluctuating pressure reduction achieved by using constant microjet pressure intensity (100 psi) along the nozzle was too dependent on the height change. In the search for some parameters expecting even noise reduction, he found that there are several parameters affecting the performance of microjet effectiveness such as microjet pressure, injection angle, the distance from lift plate to ground and nozzle pressure ratio (NPR) etc. These parameters do have an impact on the performance of the actuators and can be adjusted for the best effect under a specific nozzle condition. But the degree of effect achieved from optimally adjusted parameter is far below the desired amount and still works better only under a specific operating conditions (under-expanded case). In fact, we have another degree of freedom which was not considered in his study which is the variation of microjet intensity along the azimuthal direction.

Motivated by the above idea, in [20], we tried the experiment adjusting pressure distribution along the nozzle exit using an unique control method called "mode-matched control." It was somewhat ad hoc control strategy without considering the mechanism governing the flow and impingement tones. Fortunately, the mode-matched control strategy brought a large amount of OASPL reduction compared to the passive control method, symmetric control, had achieved. It was a very promising result because the new control strategy always showed lager reduction at all different heights and caused great amount of reduction around 9 dB where the passive control can not make any change. This is the main contribution of this thesis.

In the chapter 2, an impingement tone model called "vortex sheet model" will be presented. To implement closed-loop control in real-time, a reduced-order model of this system is needed. The model based on a vortex-sheet is discussed in chapter 2. Chapter 2 also covers a short explanation about Proper Orthogonal Decomposition(POD) method as a very useful way to capture the dominant dynamics from a model. The optimal property of POD and the practical way to implementing POD (method of snapshot) is then introduced at the end of chapter 2. In the chapter 3, the new control strategy called "mode-matched control" will be presented. The experimental result using the strategy and the noise reduction mechanism by microjet will conclude the chapter. Summary and concluding remark are presented in chapter 4.

Chapter 2

Reduced Order Model of Impingement Tone

In order to design a closed-loop control strategy, we adopt a model-based approach. A model of impingement tones, however, is quite difficult to derive due to the changing boundary conditions, compressibility effects, and the feedback interactions between acoustics and the shear-layer dynamics present in the problem. Since our primary goal is to model the impingement tone dynamics and how they respond to microjet-control action at the nozzle, we will derive a reduced-order model that only captures these dominant dynamics and the effect of control. For this derivation, while tools based on stability theory [18] can be used to obtain some of the parameters such as the tonal frequencies, they are inadequate for deriving other model-details due to the complex features of the flow field. Instead, we use the Proper Orthogonal Decomposition(POD) method and key measurements in the flow field to derive the model. This model in turn is used to derive an appropriate closed-loop control strategy.

At the beginning, this chapter will present a vortex sheet model of impingement tone and its state-space form will be suggested. At the following section, the general theory about Proper Orthogonal Decomposition(POD), a method for data compressing, and its optimality will be suggested. The theory encompasses from the definition of Karhunen-Loeve expansion and its optimality to a method of snapshot :a practical method implementing POD method. It is the summary of the some articles written

by A.J. Newman [25], L. Sirovich [36],[37],[38] and G. Berkooz [7].

2.1 Physical Model and Its State-Space Form

Model identification is one of the major tasks for designing control system and the most difficult job. In this chapter, an effort was driven to find out a suitable model for impingement system based on the previous researchers' idea. The validity of the system will be testified thorough the capability of predicting the peak in frequency domain under varying operating conditions. Based on the model, the state-space equation for control implement will also be driven.

2.1.1 Vortex Sheet Model

To control a certain physical system, it is desired to identify the mechanism governing the system. With the help from model, we can find out suitable control law and output parameter which captures the system characteristics well. That is the reason many researchers made an effort to make a plausible model of the impingement tone in spite of the difficulties.

Even though it is very difficult work to model the supersonic impinging jet due to complex phenomena such as compressibility of media or interaction between flow and acoustics, many researchers have tried to seek the proper model which mimics the real system fairly well. Previous investigators such as Wagner [44], Neuwerth [24], Ho & Nosseir [16], Umeda et al.[42] believed that the impingement tones are generated by a feedback loop. Provided energy from the instability waves in the mixing layer of the jet, instability waves are generated from acoustic wave in the region of nozzle exit. These waves magnify themselves as they are swept down to the down stream. On impinging on the ground, the acoustic waves are caused by high pressure fluctuation of the grown large scale vortical structure. According to Wagner and Neuwerth [24] the acoustic waves propagate to upstream inside the jet column for subsonic impinging jets. On the contrary, Ho & Nossier [16] suggested the propagating waves travel solely outside the jet column. However, regardless of whether the waves go inside or outside

the jet, on reaching near the nozzle exit it excites the shear layer of main jet and completes the feedback loop of noise generation.

By the feedback condition between the flow instability and the upcoming acoustic wave, the impingement frequency can be calculated from the time required for the feedback loop to complete its cycle. The impingement tone frequency f_N is determined from the following formula proposed by Powell [27]:

$$\frac{N+p}{f_N} = \int_0^h \frac{dh}{C_i} + \frac{h}{C_a} \qquad (N = 1, 2, 3, ...) \tag{2.1}$$

Here h is the distance between the wall and the nozzle exit and C_i and C_a are the convection velocities of the downstream-travelling large scale structures and the speed of upstream-travelling acoustic waves, respectively. N is an arbitrary integer and p represents a phase lag, which is caused by the phase difference between the acoustic wave and the convected disturbance at both the nozzle exit and the source of sound. Owing to the difficulty of measuring these velocities experimentally, especially in supersonic jets, most previous investigators assumed a constant value for C_i as the 60% of the main jet velocity, but it is not strictly the case. Especially at the different height, the value changes from 50 % to 60 % of the main jet velocity.

Likewise Powell, Neuwerth suggested the following relation in his paper [24]. It starts from the idea that the total number of periods in the feedback loop must be an integer.

$$\begin{aligned} h &= x\lambda_{st} = (n-x)\lambda_s \\ f &= c_a/\lambda_s = c_{st}/\lambda_{st} \end{aligned} \tag{2.2}$$

From the above equations, we can derive the following equation for the discrete frequency generated by the feedback:

$$f = \frac{n}{h(1/c_{st} + 1/c_a)} \tag{2.3}$$

h = distance between plate and nozzle aperture

n = total number of periods

x = number of vortex periods λ_{st} between plate and nozzle aperture

λ_s = acoustic wavelength

c_{st} = phase velocity of vortices

c_a = speed of sound outside jet

Similar to the role of N did in Powell's relation, an arbitrary integer n causes a staging phenomena, abrupt jump in dominant frequency as distance h changes. In the above feedback model, while the downstream instability waves is relatively well defined (Michalke [23]), the feedback acoustic wave are somewhat unclear. Wagner [44] attempted to make this wave as a plane wave. However this model was not concrete enough and some characteristics derived from the model did not support the experimental data well and moreover it couldn't predict the Strouhal number of the impingement tone with satisfactory accuracy. Ho & Nosseir's model [16] was too simple to contain any particular spatial mode structure or property either. More recently, Tam brought one model, a jet as a uniform stream bounded by a vortex sheet in his paper [40]. His trial was able to give the reason why the helical mode in large scale vortical structure was impossible for the subsonic jet flow but couldn't explain the staging phenomena at all.

In control's point of view, it is ideal to construct an exact model. But, practically, it is almost impossible to make it identical to physical system for its complexity and unexpected parameters. Hence, in this thesis, I suggest a simple model which can show one of essential characteristics, the staging phenomena because system's resonant frequency corresponding to the peak is very important in that this represents a pattern of its behavior. The objective of a plausible model of the impingement tone was to be focused on predicting the peak frequency for varying condition for the uncontrolled case and finding out the most effective and optimal control method for suppressing the noise for the controlled case.

Even though Tam's model was still insufficient in some ways, his research has

given a clue for developing the more discreet model. The model suggested in this thesis is modified version of the Tam's trial made in his paper [40]. The basic difference between Tam's model and experimental setup of Fluid Mechanics Research Laboratory in Florida State University will be mentioned afterwards.

The reduced-order model adopted for the control of impingement tones is based on the vortex-sheet jet model of [40]. Within a short distance($0.01R_j$) downstream from the nozzle exit, the jet can be idealized as a uniform stream of velocity U_j and radius R_j bounded by a vortex sheet. Small-amplitude disturbances are superimposed on the vortex sheet (see Fig. B-6). This neglects the effect of the shock structure due to the microjet action and due to underdeveloped jet (if any) and the boundary effect of the ground. Let $p_{d+}(r,\theta,z,t)$ and $p_{d-}(r,\theta,z,t)$ be the incoming pressure wave associated with the disturbances outside and inside the jet, denoted respectively by domain Ω_1 and Ω_2 where Ω_1 denotes jet-core which extends from $z=-\infty$ to $z=+\infty$, Ω_2 denotes the domain outside the jet-core and (r,θ,z) are the cylindrical coordinates. $p_{r+}(r,\theta,z,t)$ is the pressure wave reflected from lift plate. This wave has equal magnitude but opposite direction to the incoming one. Also, let $\zeta(z,\theta,t)$ be the radial displacement of the motion of a compressible flow, it can be shown that the governing equation and r-direction momentum equation for the problem are:

$$\begin{aligned} \frac{1}{a_\infty^2}\frac{\partial^2 p_{d+}}{\partial t^2} &= \nabla^2 p_{d+} \qquad (r\in\Omega_2) \\ \frac{1}{a_j^2}\left(\frac{\partial}{\partial t}+U_j\frac{\partial}{\partial z}\right)^2 p_{d-} &= \nabla^2 p_{d-} \qquad (r\in\Omega_1) \end{aligned} \tag{2.4}$$

Especially at $r=R_j$ and $z=z_{nozzle}$,

$$\begin{aligned} \frac{\partial v_+}{\partial t} &= -\frac{1}{\rho_\infty}\frac{\partial p_+}{\partial r} \\ \left(\frac{\partial}{\partial t}+U_j\frac{\partial}{\partial z}\right)v_- &= -\frac{1}{\rho_j}\frac{\partial p_-}{\partial r} \end{aligned} \tag{2.5}$$

At $r\to\infty$, p_+ satisfies the bounded condition. Where a_∞ and a_j are the speed of sound outside (Ω_2) and inside (Ω_1) the jet and U_j is the main jet speed.

Its solution is expressed as

$$\begin{bmatrix} p_{d+}(r,z,\theta,t) \\ p_{d-}(r,z,\theta,t) \\ \zeta(z,\theta,t) \end{bmatrix} = \begin{bmatrix} \hat{p}_{d+}(r) \\ \hat{p}_{d-}(r) \\ \hat{\zeta} \end{bmatrix} e^{i(kz+n\theta-\omega t)} \tag{2.6}$$

where $n = 0, \pm 1, \pm 2,...$ and k, the wavenumber and ω (ω>0), the angular frequency are as yet unspecified parameter. Substituting the solution (2.6) into (2.4), it leads to the following eigenvalue problem about $\hat{p}_{d+}$ and $\hat{p}_{d-}$:

$$\frac{d^2\hat{p}_{d+}}{dr^2} + \frac{1}{r}\frac{d\hat{p}_{d+}}{dr} - \frac{n^2}{r^2}\hat{p}_{d+} + \left[\frac{\omega^2}{a_\infty^2} - k^2\right]\hat{p}_{d+} = 0 \tag{2.7}$$

$$\frac{d^2\hat{p}_{d-}}{dr^2} + \frac{1}{r}\frac{d\hat{p}_{d-}}{dr} - \frac{n^2}{r^2}\hat{p}_{d-} + \left[\frac{(\omega - U_j k)^2}{a_j^2} - k^2\right]\hat{p}_{d-} = 0 \tag{2.8}$$

The solutions of (2.7) and (2.8) give

$$\hat{p}_{d+} = C_1 H_n^{(1)}(\eta_+ r) \tag{2.9}$$

$$\hat{p}_{d-} = C_2 J_n(\eta_- r) \tag{2.10}$$

where $H_n^{(1)}$ is the n^{th} order Hankel function of the first kind, J_n is n^{th} order Bessel function of the first kind, $\eta_+ = (\omega^2/a_\infty^2 - k^2)^{\frac{1}{2}}$, $\eta_- = \left[(\omega - U_j k)^2/a_j^2 - k^2\right]^{\frac{1}{2}}$ and C_1 and C_2 are unknown constants which are to be determined from boundary conditions.

Tam, in his paper, mentioned the necessary boundary conditions that make the problem well-posed, are as follows.

- Dynamic condition $r = R_j$:

$$p_+ = p_- \tag{2.11}$$

- Kinematic condition $r = R_j$:

$$v_+ = v_-$$

This is definitely a necessary requirement for his model. As seen in Fig. B-6, the impingement tone system of his paper is different from the experimental setup of Fluid Mechanics Research Laboratory in Florida State University in that Tam's model does not have a lift plate which makes the problem more complicated. In reality, the shear layer near the nozzle is usually excited from the acoustic wave generated from downstream mixing layer. In addition to these direct influences, it is excited by the bouncing acoustic wave from the lift plate near the nozzle exit too. These direct and reflected acoustic wave intensify the flow interaction with it and magnify the excitation of the shear layer more violently than simple nozzle without lift plate. Hence, the previous dynamic and kinematic equality condition are should be modified especially at near the nozzle exit as:

Condition 1 Dynamic condition $r = R_j$:

$$p_+ - p_- = \Delta p\, \delta(z-\epsilon) e^{i(n\theta-\omega t)} \tag{2.12}$$

where p_+ represents the outside pressure field, the superposition of the acoustic wave (p_{d+}) travelling upstream, and a wave reflected from lift plate (p_{r+}) propagating in the opposite direction with an equal magnitude, i.e., $p_{r+}(r,\theta,z,t) = p_{d+}(r,\theta,-z,t)$. p_- represents the inner pressure field inside the main jet, and Δp denotes an imposed pressure jump across the shear layer.

Condition 2 Kinematic condition $r = R_j$:

$$v_+ - v_- = \Delta v\, \delta(z-\epsilon) e^{i(n\theta-\omega t)} \tag{2.13}$$

where v_+ represents the outside radial velocity field, v_- represents the inner radial velocity field and Δv represents an imposed velocity jump across the shear layer.

Mathematically, the pressure field in the entire flow field can now be expressed as follows.

$$\begin{aligned} p_+ &= p_{d+} + p_{r+} \\ &= A_1 H_n^{(1)}(\eta_+ r) cos(kz) e^{i(n\theta-\omega t)} \qquad (2.14) \\ p_- &= A_2 J_n(\eta_- r) cos(kz) e^{i(n\theta-\omega t)} \qquad (2.15) \end{aligned}$$

where constant A_1 and A_2 are to be obtained from boundary conditions.

The pressure and velocity jump Δp and Δv are imposed due to the presence of the ground plane and can be determined as follows. We model the ground effect by introducing 'virtual' acoustic sources on the ground plane. In particular, infinite number of monopoles are assumed to be present at $z = L$, along a circular line of radius $r = R_j$, with strength S_w varying along the azimuthal coordinate θ. The source strength is the influenced by the jet vortical structures impinging on the ground plane and is assumed as

$$S_w(\theta) = \kappa p_+(r = R_j, \theta, z = L) \tag{2.16}$$

where κ is a proportional constant whose value can be estimated by comparison with the experimental data (see Fig. B-7). Using equation. (2.16) and Fig. B-7, we then calculate Δp and Δv from the sum of pressure excitation caused by each monopole:

$$\begin{aligned} \Delta p\, e^{i(n\theta_1 - \omega t)} &= \int_0^{2\pi} \Delta p_{monopole}(\theta; \theta_1) d\theta \\ &= \int_0^{2\pi} S_w(\theta; n) \left(-\rho_j \frac{\partial \phi_{monopole}}{\partial t} \right) d\theta \end{aligned} \tag{2.17}$$

and

$$\Delta v\, e^{i(n\theta_1 - \omega t)} = \int_0^{2\pi} \nabla \phi_{monopole} d\theta \tag{2.18}$$

where θ_1 is the azimuthal location of interest, $\Delta p_{monopole}(\theta; \theta_1)$ is the pressure excitation at the collecting point (θ_1) on the lift plate due to a monopole placed at θ of the ground plane, $\phi_{monopole}$ is the velocity potential due to each monopole placed on ground plane, and ρ_j is the density of medium in the jet nozzle. The velocity potential in a moving media can be expressed as[13]

$$\phi = 2\pi \frac{exp\left\{ -i\omega t - \dfrac{i\omega M_1 z}{1 - M_1^2} + \dfrac{i\omega}{c\,(1 - M_1^2)^{0.5}} \left(\dfrac{z^2}{1 - M_1^2} + x^2 + y^2 \right)^{0.5} \right\}}{(1 - M_1^2)^{0.5} \left(\dfrac{z^2}{1 - M_1^2} + x^2 + y^2 \right)^{0.5}}. \tag{2.19}$$

where ω is frequency of acoustic wave in radian, c is sound speed and M_1 is the Mach number of moving media. Therefore equation (2.17), (2.18) become

$$\Delta p\, e^{in\theta_1} = \int_0^{2\pi} \frac{2\pi i \rho_j \omega S_w(\theta;n)}{l(\theta;\theta_1)} \frac{exp\left\{-\dfrac{i\omega M_1 L}{1-M_1^2} + \dfrac{i\omega}{c\left(1-M_1^2\right)^{0.5}} l(\theta;\theta_1)\right\}}{\left(1-M_1^2\right)^{0.5}} d\theta \tag{2.20}$$

$$\Delta v\, e^{in\theta_1} = \int_0^{2\pi} -\frac{2\pi S_w(\theta;n)}{l^{5/2}(\theta;\theta_1)} \{r - R_j\cos(\theta_1-\theta)\} \frac{exp\left\{-\dfrac{i\omega M_1 L}{1-M_1^2} + \dfrac{i\omega}{c\left(1-M_1^2\right)^{0.5}} l(\theta;\theta_1)\right\}}{\left(1-M_1^2\right)^{0.5}} d\theta \tag{2.21}$$

where L is the distance between lift plate and ground plane and l is defined as

$$l = \sqrt{\frac{L^2}{1-M_1^2} + 2R_j^2 - R_j^2\cos(\theta_1-\theta)}.$$

To determine A_1 and A_2, three additional conditions due to geometrical restrictions are imposed near the lift plate and ground plane:

Condition 3 The zero normal flow condition on the lift plate is:

$$\frac{\partial p_+}{\partial n} = 0 \qquad (r \in \Omega_2, z = z_{nozzle}) \tag{2.22}$$

Aside from these flow condition, Tam's model omitted another important factor affecting the mechanism. In his work, the distance between lift plate to ground plane does not do any crucial contribution on distinct noise frequency. One of the conspicuous result of the supersonic impinging tone is the staging phenomena of dominant frequency in acoustic tone. Referring from previous data in fig[B-18], the staging phenomenon can be concluded to be strongly dependant to the relative distance between lift plat and ground plane. In general, the gap between two plate influence on change of dynamics mostly by changing main jet speed. Elavarasan et al. [11] measured the centerline velocity variation along the supersonic main jet in Fig. B-16. In this experiment, he tried to suppress the amount of sound by blocking the upcoming wave using baffle near the nozzle exit. As a byproduct he measured centerline

velocity with and without baffle. Without any control effect, the centerline velocity can be considered almost constant all the way from lift plate to ground plane except impingement region. Motivated by the experimental result, such flow variation was introduced to the Tam's model. The centerline flow is treated to be constant except impinging region where its velocity decreases suddenly to zero, which is idealized in Fig. B-16 and another condition is added as follows.

Condition 4 Mean velocity condition of main jet (see Fig. B-16) is assume to be of the form

$$U_j = \begin{cases} U_0 & : \quad 0 < z < 0.8L \\ -\dfrac{U_0}{0.2L} z + 5U_0 & : \quad 0.8L < z < L \end{cases}$$

where U_0 is the exit velocity corresponding to a given Mach number M_1.

Condition 4 is inspired from experiments done by Krothapalli et al. [19], where the mean centerline velocity of impinging jet was observed to drastically reduce to zero near the ground plane. The centerline velocity model is idealized as Fig. B-16.

Condition 5 Equality condition at r = R_j without microjet:

$$\begin{aligned} \frac{\partial v_+}{\partial t} &= -\frac{1}{\rho_\infty}\frac{\partial p_+}{\partial r} \\ \left(\frac{\partial}{\partial t} + U_j \frac{\partial}{\partial z}\right) v_- &= -\frac{1}{\rho_j}\frac{\partial p_-}{\partial r}. \end{aligned} \tag{2.23}$$

Substituting equation (2.14) into (2.12) and (2.13) together with (2.23), **Conditions 1** and **2** can be written as

$$\left[A_1 H_n^{(1)}(\eta_+ R_j) - A_2 J_n(\eta_- R_j)\right] \cos(kz) = \Delta p \delta(z - \varepsilon) \tag{2.24}$$

and

$$\frac{1}{i\omega\rho_\infty}\frac{\partial p_+}{\partial r} - \frac{1}{i(\omega - U_j k)\rho_j}\frac{\partial p_-}{\partial r} = \Delta v \delta(z - \varepsilon). \tag{2.25}$$

Integrating the above equation in the range of $(0 < z < L)$, we get

$$\frac{A_1 H_n^{(1)}(\eta_+ R_j)\sin(kL)}{k} - \int_0^L \{A_2 J_n(\eta_- R_j)\cos(kz)\}dz = \Delta p \tag{2.26}$$

and

$$\left\{\frac{1}{i\omega\rho_\infty} A_1 H_n^{'(1)}(\eta_+ R_j)\eta_+\right\}\frac{\sin(kL)}{k} - \int_0^L \left\{\frac{1}{i(\omega - U_j k)\rho_j} A_2 J_n^{'}(\eta_- R_j)\eta_-\right\}\cos(kz)dz = \Delta v. \tag{2.27}$$

Then the pressure amplitude can be calculated from the following equation:

$$\begin{bmatrix} A_1 \\ A_2 \end{bmatrix} = \frac{1}{F_{11}F_{22} - F_{12}F_{21}} \begin{bmatrix} F_{22} & -F_{12} \\ -F_{21} & F_{11} \end{bmatrix} \begin{bmatrix} \Delta p \\ \Delta v \end{bmatrix} \tag{2.28}$$

where

$$F_{11} = H_n^{(1)}(\eta_+ R_j)\frac{\sin(kL)}{k},$$

$$F_{12} = -\int_0^L \{J_n(\eta_- R_j)\cos(kz)\}\, dz,$$

$$F_{21} = \left\{\frac{1}{i\omega\rho_\infty} H_n^{(1)'}(\eta_+ R_j)\eta_+\right\}\frac{\sin(kL)}{k}, \text{ and}$$

$$F_{22} = \int_0^L \left\{\frac{-1}{i(w - U_j k)\rho_j} J_n^{'}(\eta_- R_j)\eta_-\right\}\cos(kz)dz.$$

Equations (2.14), (2.17), (2.18), and (2.28) provide the complete solution to the governing equations of the impingement tones problem, given by equation (2.4).

2.1.2 A Control-Oriented Model

As mentioned in the introduction, the goal is to reduce the impingement tones using a suitable active flow control method. In the experimental facility, active flow control was implemented using sixteen microjets that are flush mounted circumferentially around the main jet nozzle. The question here is to determine a control strategy for modulating the microjet pressure profile in an optimal manner.

In order to determine the control strategy, the effect of the microjet has to be incorporated into the model. We note that when microjets are introduced into the main jet, **Condition 5** is changed at $z = z_{nozzle}$, since an additional velocity u_μ is added due to the microjet action. We therefore introduce yet another

Condition 6 Equality condition at r = R_j with microjet:

$$\begin{aligned} \frac{\partial v_+}{\partial t} &= -\frac{1}{\rho_\infty}\frac{\partial p_+}{\partial r} \\ \left(\frac{\partial}{\partial t} + U_j\frac{\partial}{\partial z} - u_\mu \sin\alpha\frac{\partial}{\partial r}\right) v_- &= -\frac{1}{\rho_j}\frac{\partial p_-}{\partial r} \end{aligned} \tag{2.29}$$

where u_μ is the microjet velocity and α is the microjet inclination angle with respect to the nozzle center line. The overall solution for A_1 and A_2 can be derived in a similar manner as before, using **Conditions 1** through **6**.

2.1.3 Model Validation

We now validate the model described in the previous section using the experimental results obtained from the STOVL supersonic jet facility of the Fluid Mechanics Research Laboratory (FMRL) located at the Florida State University [1]. For the sake of completeness, we briefly describe the facility below (see Fig. B-4 and B-5 for a schematic).

The measurements were conducted using an axisymmetric, convergent-divergent (C-D) nozzle with a design Mach number of 1.5. The throat and exit diameters (d, d_e) of the nozzle are 2.54cm and 2.75cm (see Figs. B-4 and B-5).

The divergent part of the nozzle is a straight-walled conic section with a 3^o divergence angle from the throat to the nozzle exit. A circular plate of diameter D (25.4cm $\sim$ $10d$) was flush mounted with the nozzle exit, which represents the 'lift plate' of a generic aircraft planform and has a central hole, equal to the nozzle exit diameter, through which the jet is issued. A 1m $\times$ 1m $\times$ 25mm aluminum plate serves as the ground plane and is mounted directly under the nozzle on a hydraulic lift, and arranged so that the height h of the lift plate from the ground plane can

be varied over a desired range. To validate the model, this facility was run at Mach 1.5, at h/d = 3.0, 4.0, and 4.5. The detailed information about the experimental condition will be mentioned the following chapter.

From equation (2.28), it is clear that the peak in the pressure data is determined by the set (ω,k) which satisfies the denominator $F_{11}F_{22} - F_{12}F_{21} = 0$. The solution to this equation is not unique and we choose that particular value of (ω,k) which corresponds to a phase velocity equal to the ambient speed of sound. This means that the upstream propagating acoustic wave outside the jet has a phase velocity same as that of the speed of sound in air at rest.

Using equation (2.17), (2.18), and (2.28), the solution p^+ is compared to the actual experimental data in Fig. B-17 for the first azimuthal mode, n =1, at the lift plate.

It is clear that the prediction of amplitude of the pressure signal by the model is poor. This may be due to the fact that the velocity potential in equation (2.19) is assumed to contain no damping effects. Therefore, no further insight can be obtained by comparing the amplitude of predicted pressure spectrum with that observed from experiments in Fig. B-17.

Henceforth, we focus on the ability of the model to predict the frequency of impingement tones for different h/d ratios. It was observed that the peak frequency calculated from the analytical model shows "staging" phenomena similar to the experimental data. Fig. B-18 shows a comparison of the staging phenomenon of impingement tones between data obtained through the model and experiments. It is encouraging to observe that each tone decreases in frequency approximately linearly with increase in h/d. Note that in Fig. B-18(a), the dominant frequencies observed in the experiment closely match the edge tones[27] given by the well-known relation

$$\frac{N+\varphi}{f_N} = \int_0^h \frac{dh}{C_i} + \frac{h}{C_a} \qquad (N = 1, 2, 3, ...) \tag{2.30}$$

where C_i and C_a are the convective velocities of the downstream-travelling large structures and the speed of upstream-travelling acoustic waves, respectively, for a suitably chosen N and p.

The other relevant parameter that the model predicts is the frequency interval

between two tones for different h/d ratios. The result is summarized in Table A.2. It is again encouraging to note that the modelling error relative to the experimental data is less than 20%.

Figs. B-15 and B-19 show the peak frequency intervals between experimental and modelling results at a particular height, $h/d = 6.0$.

Clearly, Δf_1 and Δf_2 are comparable in the two figures. It can also be observed from Table A.2 and Fig. B-19 that the peak interval in both the experimental data and the analytical solution decreases as the height of the lift plate from the ground plane increases from $h/d = 2.0$ to $h/d = 5.0$. This behavior is not observed beyond $h/d = 5.0$ and can be attributed to varying dynamics governing the impingement tones with height. When the lift plate is close enough to the ground plane, the upstream propagating acoustic waves due to impingement plays a major role in shear layer excitation but its effect diminishes at larger distances. Moreover, the error between the experimental peak interval and predicted one is almost less than 20% at every h/D and is around 6% at heights where the feedback loop is a dominant mechanism in noise generation.

As far as we know, the present work is among the first to obtain analytical models of impingement tones predicting the staging phenomenon and frequency interval magnitudes within tolerable limits. Although the two are not sufficient indicators of the validity of this model, yet the model is considered sufficiently rich and reliable enough to be suitably used as a mathematical model for obtaining control strategy that results in optimal noise reduction.

2.1.4 State-Space Equations

So far, we have sought for a model without microjet control and shown the validity from its ability to predict peak frequency interval for different heights. Regarding the model as a fairly good enough, model-based control strategy still requires a complete state-space equation with well defined input and output factor. One major contribution the microjet can make is velocity change in radial direction near the nozzle exit. Introduction of microjets disturbs the vortex sheet and its effect can be represented

by the modified momentum equation in r-direction (2.23) as follows:

At $r = R_j$, $z = z_{nozzle}$

$$\begin{aligned} \left(\frac{\partial}{\partial t} + u_\mu(p_\mu)\frac{\partial}{\partial z}\right) v_+ &= -\frac{1}{\rho_\infty}\frac{\partial p_+}{\partial r} \\ \left(\frac{\partial}{\partial t} + (U_j + u_\mu(p_\mu))\frac{\partial}{\partial z}\right) v_- &= -\frac{1}{\rho_j}\frac{\partial p_-}{\partial r} \end{aligned} \tag{2.31}$$

where u_μ is the amount of radial directional velocity increase by microjet injection, p_μ is the supply pressure to microjet.

By separation of variables, we can write for the outer area Ω_2:

$$p_+(r, \theta, z, t) = \sum_{i=1}^{L} X_i(t)\Phi_i(r, \theta, z) \tag{2.32}$$

where X_i is the state variable, Φ_i is a set of orthonormal functions satisfying the boundary conditions (**Condition 1** $\sim$ **Condition 5**) and hence can be viewed as the first L modes of the system. Clearly, Φ_i is a function of microjet pressure p_μ. Substituting in equation (2.4), and taking inner product with respect to Φ_i, we get:

$$\ddot{X}_j(t) = a_\infty^2 \sum_{i=1}^{l} (\nabla^2\Phi_i, \Phi_j)X_i(t) \qquad j = 1, \cdots, L \tag{2.33}$$

Since the modes are dependant upon p_μ, we can write equation (2.32) in vector form as:

$$\dot{X}(t) = A(p_\mu)X(t) \tag{2.34}$$

Discussion about state-space form will stop here. More discrete construction of matrix $A(p_\mu)$ will be treated at ongoing research. Till now we derived state-space form, essential expression of governing equation, and confirmed that this is different from conventional one in that the control input parameter appears as a parameter in matrix A rather than independent term. The detailed control strategy will be exploited at the next chapter.

2.2 Proper Orthogonal Decomposition

From several different engineering fields, a lot of system's behaviors are governed by mathematical formula such as ordinary differential equation or partial differential equation. Many types of physical system are well represented by the solution to these equations. For example, in fluid mechanics field, flow field is fairy well predicted under Navier-Stokes equation. Hence, to get a solution characterizing the detailed motion as close to the real system as possible has been one of the major objective to Fluid mechanics field.

But that is not the sole objective in formulating mathematical model for dynamical system. In case you are trying to control a plat under the real-time condition, solution to a particular case is not meaningful under different situation. Real-time control requires a short calculation time rather than the exact solution. Hence it is needed to sacrifice the correctness of model for making the equation easier to solve and shorten the computation time.

The Proper Orthogonal Decomposition (POD) is a tool used to extract the most energetic modes from a set of realization from the underlying system [17]. These modes can be used as basis functions for Galerkin projections of the model in order to reduce the solution space being considered to the smallest linear subspace that is sufficient to describe the system. The decomposition is 'optimal' in that the energy contained in an N-ordered POD base is greater than any other N-ordered base in a mean-squared sense. Over the years, it has been applied in several disciplines including turbulence in fluid mechanics, stochastic processes, image processing, signal analysis, data compression, process identification and control in chemical engineering, and oceanography, and has been referred to by various names including Karhunen-Loeve decomposition, principal component analysis, and singular value decomposition. In fluid mechanical systems, the POD technique has been applied in the analysis of coherent structures in turbulent flows and in obtaining reduced order models to describe the dominant characteristics of the phenomena. One of the earliest works was on a fully developed pipe flow, studied by Bakewell and Lumley [6]. Since then,

POD models have been used to model the one-dimensional Ginzburg-Landau equation (Sirovich and Rodriguez [39]), the laminar-turbulent transitional flow in a flat plate boundary layer (Rempfer [30]), pressure fluctuations surrounding a turbulent jet (Arndt et al. [4]), turbulent plane mixing layer (Delville et al. [10]), velocity field for an axisymmetric jet (Citriniti and George [9]), low-dimensionality of a turbulent flow near wake (Ma et al. [22]), low-dimensional leading-edge vortices in the unsteady flow past a delta wing (Cipolla et al. [8]), and flow over a rectangular cavity (Rowley et al. [31]). The eigenfunctions were developed using both experimental and numerical database.

2.2.1 The Karhunen-Loeve Expansion

Suppose a flow is defined on a spatial domain Ω during a time interval T, the flow behaviors such as velocity, trajectory and pressure can be determined from governing equation. These prediction guarantees the accuracy only when the information about boundary condition and initial condition are perfectly given and the governing equation mimics the real system fairly well. But at a certain case the flow field is too sensitive to boundary condition and the small perturbation is not easily detected using a sensor, conventional deterministic flow expression becomes useless. To avoid the unpredictability, the flow is treated as a random process with parameter of time and space. We shall denote the flow variable as follows:

$$\{u_{t,x}; t \in [0, \infty), x \in \Omega\} \tag{2.35}$$

Suppose a flow variable is expressed the sum of orthonormal basis $a(t)$ and $\phi(x)$,

$$u(x,t) = \sum_{n=1}^{\infty} a_n(t)\phi_n(x). \tag{2.36}$$

the complexity of the model can be reduced by truncating the series at a suitable value. There are a large number of basis set to construct the flow, for example equation (2.36). Among these, the Karhunen-Loeve expansion is also one way to

decompose a signal into infinite sum of spatial and temporal term aiming to reduce the complexity.

Mathematically speaking, the flow expanded using the Karhunen-Loeve theorem is stated that,

$$u(t,x) = \sum_{n=1}^{\infty} \sqrt{\lambda_n} a_n(t) \phi_n(x) \tag{2.37}$$

where the temporal terms are uncorrelated

$$\begin{aligned} a_n(t) &= (\sqrt{\lambda_n})^{-1} \int_\Omega \phi_n(x) u(t,x) dx \\ E[a_m(t) a_n(t)] &= \delta_m^n \qquad (2.38) \\ \int_\Omega \phi_n(x) \phi_n(x) dx &= \delta_m^n \qquad (2.39) \end{aligned}$$

and the orthonormal basis functions $\{\phi_n\}$ are calculated from integral equation based on covariance function $R_u(x,y)$

$$\begin{aligned} &\int_\Omega R_u(x,y) \phi_n(y) dy = \lambda_n \phi_n(x) \qquad x \in \Omega \\ &R_u(x,y) = E[(u_x - \mu(x))(u_y - \mu(y))] \end{aligned} \tag{2.40}$$

where $\mu(x), \mu(y)$ are mean values of variable u_x, u_y, respectively and $\delta_m^n = 0$ (if $m \neq n$), 1 (if $m = n$) . The derivation of the temporal term, the uncorrelated property and more rigorous proof can be found in Newman's paper [25].

2.2.2 Optimality of the Karhunen-Loeve Expansion

Karhunen-Loeve expansion is the optimal linear decomposition method for variables. Here, the "optimal" means that the projection of a variable on the POD mode (kinetic energy in flow variable sense) is greater than the projection on any other linear decomposition in an average sense for a given number of modes. In other words, Karhunen-Loeve expansion has the least time-averaged error to the original data. Brief explain about optimality will be mentioned here. For the more rigorous proof, it would be better refer to the previous work conducted by Berkooz et al.[7]. If a single

mode $\{\phi\}$ is said to be "similar" to a variable u, it can be expressed mathematically as follows.

$$\max_{\psi} \langle |(u,\psi)|^2 \rangle / (\psi,\psi) = \langle |(u,\phi)|^2 \rangle / (\phi,\phi) \tag{2.41}$$

As to Berkooz et al.[7], a necessary condition for the equation (2.41) to hold is that ϕ is an eigenvalue of the two-point correlation function.

$$\int_{\Omega} \langle u(x), u^*(x') \rangle \phi(x') dx' = \lambda \phi(x') \tag{2.42}$$

$(f,g) = \int_{\Omega} f(x) g^*(x) dx$: inner product

$\langle\ ,\ \rangle$: time, space or phase average

$R(x,x') = \langle u(x), u(x') \rangle$: two-point correlation tensor

Then, the solution ϕ satisfying the equation (2.42) will maximize the equation (2.41). But the above eigenvalue problem has infinite number of solutions as long as Ω is bounded. We can normalize these eigenfunctions $\{\phi_k\}$ so that $\|\phi_k\| = 1$ and order their eigenvalues by $\lambda_n \geq \lambda_{n+1} \cdots \geq 0$

If a flow signal u can be decomposed with respect to the POD orthonormal basis set, it is given by

$$u(x,t) = \sum a_n(t) \phi_n(x). \tag{2.43}$$

In Newman's paper [25], it is shown that the mean energy of the flow projected on the a specific mode corresponds to the eigenvalue λ_n

$$\begin{aligned}
E[|(\phi_n, u)|^2] &= E[|\int \phi_n(x) u(t,x) dx|^2] \\
&= E[\int \phi_n(x) u(t,x) dx \int \phi_n(y) u(t,y) dy] \\
&= E[\int \int \phi_n(x) u(t,x) \phi_n(y) u(t,y) dy dx] \\
&= \int \int \phi_n(x) E[u(t,x) u(t,y)] \phi_n(y) dy dx \\
&= \int \phi_n(x) \int R(x,y) \phi_n(y) dy dx \\
&= \int \phi_n(x) (\lambda_n \phi_n(x)) dx
\end{aligned}$$

$$
\begin{aligned}
&= \lambda_n \int |\phi_n(x)|^2 dx \\
&= \lambda_n
\end{aligned} \tag{2.44}
$$

and the POD coefficient are uncorrelated

$$\langle a_n(t), a_m^*(t) \rangle = \delta_n^m \lambda_n. \tag{2.45}$$

From the above equation (2.44), (2.45) and (2.41), the kinetic energy per unit mass over the domain is denoted by

$$\int_\Omega \langle u, u^* \rangle dx = \sum_{n=1}^{N} \langle a_n, a_n^* \rangle = \sum_{n=1}^{N} E[|(\phi_n, u)|^2]. \tag{2.46}$$

Suppose the flow signal is expressed from other arbitrary orthonormal set ψ,

$$
\begin{aligned}
u(x,t) &= \sum b_n(t)\psi_n(x) \\
\int_\Omega \langle u, u^* \rangle dx &= \sum_n \langle b_n, b_n^* \rangle
\end{aligned} \tag{2.47}
$$

According to the equation (2.41), its energy content projected by a mode ψ is always less than that by POD mode ϕ.

$$\sum_{n=1}^{N} \langle a_n(t), a_n^*(t) \rangle = \sum_{n=1}^{N} E[|(\phi_n, u)|^2] = \sum_{n=1}^{N} \lambda_n \geq \sum_{n=1}^{N} E[|(\psi_n, u)|^2] = \sum_{n=1}^{N} \langle b_n(t), b_n^*(t) \rangle \tag{2.48}$$

Therefore, among all linear decompositions, Karhunen-Loeve expansion contains the most energy possible for a given number of modes, which fosters POD method to be used as a good way for reconstructing the model the most efficiently.

There are other approach to explaining the optimality. If $F(x,t)$ is a generalized zero-mean flow variable, then the POD method seeks to generate an approximation for F by using separation of variables as

$$\hat{F}(x,t) = \sum_{i=1}^{l} T_i(t)\phi_i(x) \tag{2.49}$$

where $T_i(t)$ is the i^{th} temporal mode, $\phi_i(x)$ is the i^{th} spatial mode, l is the number of modes chosen, and t and x are the temporal and spatial variables respectively. The

POD method consists of finding ϕ_i such that the error $F(x,t) - \hat{F}(x,t)$ is minimized. This optimization problem can be stated as follows.

Denote $\{\phi_i(x)\}_{x=x_1,\cdots,x_n} = \bar{\phi}_i \in \Re^n$. The POD method is the following optimization problem:

$$\min_{\Psi} J_m(\bar{\phi}_1, ..., \bar{\phi}_l) = \sum_{j=1}^{m} \|Y_j - \sum_{k=1}^{l} (Y_j^T \bar{\phi}_k)\bar{\phi}_k\|^2 \tag{2.50}$$

subject to :

$$\bar{\phi}_i^T \bar{\phi}_j = \delta_{ij},\ 1 \leq i,j \leq l, \Psi = [\bar{\phi}_1, ..., \bar{\phi}_l] \tag{2.51}$$

where $Y_j \in \Re^n$ is the vector of flow data F at time $t = t_j$.

By definition [43], Ψ is a POD modal set if it is a solution to the optimization problem (2.50) for any value of $l \leq m$.

2.2.3 Method of Snapshots

In practice, flow data are measured from a form of discrete signal by a transducer. The analogous form of the Karhunen-Loeve expansion should be calculated from infinite sum of each terms. The procedure for calculating the analogous Karhunen-Loeve expansion is summarized as follows.

1. Let $\{u_i(t)\}$ be a flow variable of a distinct position i at time t

2. The $i,j'th$ element of the covariance matrix $(R)_{ij}$ is given by $E[u_i, u_j]$ and the corresponding orthonormal eigenvector ϕ and λ are calculated from

$$R\phi_n = \lambda_n \phi_n \qquad n = 1, 2, 3 \cdots \tag{2.52}$$

3. The analogous Karhunen-Loeve expansion and its corresponding temporal term is derived:

$$\begin{aligned} u_i(t) &= \sum_{n=1}^{\infty} \sqrt{\lambda_n} a_n(t)(\phi_n)_i \\ a_n(t) &= (\sqrt{\lambda_n})^{-1} \sum_{i=1}^{\infty} (\phi_n)_i u_i(t) \end{aligned} \tag{2.53}$$

Above procedure for obtaining analogous Karhunen-Loeve expansion is reasonable but very impractical due to infinite sum. It might cause serious computation problem especially for treating a large number of spatial data. If the number of discrete spatial points might increase, the dimension of the covariance matrix R increases fast that the required computation time to get the eigenvalue also extremely longer. Consider a vary coarse lattice, even $10 \times 10 \times 10$ division renders the 1000×1000 size covariance matrix. It is very ineffective in practical points of view. The difficulties associated with large data set should be avoided.

Sirovich [36] in his paper mentioned the method of snapshots, a nice way to make the calculation more simple and the computation less burdensome. Newman [25] showed the detailed derivation of the snapshot method which gives great advantages from the practical points of view. The following is the procedure to get the eigenvectors empirically.

Practically, the continuous flow $u(t,x)$ is expressed by $u^n = u(n\tau, x)$ where τ is the time interval between data collection. The ergodic hypothesis gives the correlation function as

$$R(x,y) = \lim_{T\to\infty} \frac{1}{T} \int_0^T u(x,t)u(y,t)dt \tag{2.54}$$

and in the same manner, for the sufficiently large M, it can be approximated as

$$\tilde{R}(x,y) = \frac{1}{M} \sum_{n=1}^{M} u^{(n)}(x)u^{(n)}(y) \tag{2.55}$$

The integral operator of the approximation becomes

$$\begin{aligned} \int_\Omega \tilde{R}(x,y)\phi(y)dy &= \int_\Omega \frac{1}{M} \sum_{n=1}^{M} u^{(n)}(x)u^{(n)}(y)\phi(y)dy \\ &= \frac{1}{M} \sum_{n=1}^{M} u^{(n)}(x) \int_\Omega u^{(n)}(y)\phi(y)dy \\ &= \sum_{n=1}^{M} \alpha_n u^{(n)}(x) \end{aligned} \tag{2.56}$$

From the equation (2.40), this value should satisfy the following

$$\sum_{n=1}^{M} \alpha_n u^n(x) = \lambda\phi(x) \tag{2.57}$$

Therefore, the empirical eigenfunction can be written

$$\phi(x) = \sum_{n=1}^{M} A_n u^n(x) \tag{2.58}$$

Substituting this result to the equation (2.55),

$$\begin{aligned} \int_\Omega \frac{1}{M} \sum_{n=1} M u^{(n)}(x) u^{(n)}(y) \sum_{m=1} M A_m u^{(m)}(y) dy &= \lambda \sum_{n=1}^{M} A_n u^n(x) \\ \frac{1}{M} \sum_{n=1} M u^{(n)}(x) \sum_{m=1} M A_m \int_\Omega u^{(n)} u^{(m)}(y) dy &= \lambda \sum_{n=1}^{M} A_n u^n(x) \end{aligned} \tag{2.59}$$

Finally, it is represented as a matrix form

$$(CA)^T V = \lambda A^T V \tag{2.60}$$

where the matrix C is defined by

$$\begin{aligned} &C_{ij} = \frac{1}{M} \int_\Omega u^{(i)}(x) u^{(j)}(x) dx, \\ &A = [A_1, \cdots, A_M]^T, \qquad V = [u^{(1)}(x), \cdots, u^{(M)}(x)]^T \end{aligned} \tag{2.61}$$

Accepting that the Grammian

$$\int_\Omega V(x) V^T(x) dx \tag{2.62}$$

is positive definite, $(CA)^T V(x) = \lambda A^T V(x)$ hold if and only if $CA = \lambda A$. Therefore, the solutions to (2.55) are equivalent to solutions of

$$CA = \lambda A \tag{2.63}$$

Note that that quality of the approximation depends on the number of data samples. High spatial resolution might contribute the computation time but this is the inner products of equation (2.61). This computation involves only add-multiply operation is of minor importance in an actual calculation.

Tang et al. [41] suggested a simple way to get the POD mode by doing matrix calculation. Let the $p^n(j)$ be the pressure variable at a spatial point n at some time j where n = 1,2,$\cdots$,N and j = 1,2,$\cdots$,J, with n much smaller than J usually. Now the matrix Q can be expressed from singular value decomposition as

$$Q = \begin{pmatrix} p^1(1) & p^1(1) & \cdots & p^1(J) \\ p^2(1) & p^2(1) & \cdots & p^2(J) \\ p^3(1) & p^3(1) & \cdots & p^3(J) \\ \vdots & \vdots & \cdots & \vdots \\ p^N(1) & p^N(1) & \cdots & p^N(J) \end{pmatrix} = U\Sigma V^T$$

where $U(N \times l)$ and $V(J \times l)$ are unitary matrix

$$[U]^T[U] = [I]_{l\times l}, \qquad [V]^T[V] = [I]_{l\times l} \tag{2.64}$$

and

$$[\Sigma]_{l\times l} = \begin{pmatrix} \sigma_1 & & & & \\ & \sigma_2 & & & \\ & & \cdot & & \\ & & & \cdot & \\ & & & & \sigma_l \end{pmatrix}$$

$$\sigma_1 \leq \sigma_2 \leq \sigma_3 \leq \cdots \sigma_l \tag{2.65}$$

The matrix V and σ are the eigenvector and the square-root of the eigenvalue of the correlation matrix Q^TQ each. The mode-shape can be computed by normalizing each column of the following matrix Φ.

$$\Phi \equiv QV = [\phi_1 \quad \phi_2 \cdots \phi_l]. \tag{2.66}$$

In short, the spatial i^{th} POD mode can be obtained as given below:

$$\phi_i(x_n) = \sum_{j=1}^{m} \frac{V(j,i)Q(x_n,j)}{\sigma_i} \tag{2.67}$$

Chapter 3

POD-based Closed-loop Control Strategy

The aim of the research is to reduce OASPL at several heights using the pressure information of the lift plate. As seen at the previous chapter, the impingement tones and the ambient flow field are generated from complicated mechanism and the governing equation describing the impinging tone can not be considered as perfect. Hence, model based closed-loop control can not guarantee better performance yet. For the time being, we have to rely on the measured data to infer the governing mechanism. But measurement based control strategy also has some drawbacks in that we can not get full information of flow field and measurable properties are are confined on only the pressure of lift plate. Moreover, pressure data also requires to be processed in a short time to be feeded into the control input. From those reason, it is necessary to capture the dominant dynamics governing impingement tone. To extract the information as much as possible without losing dominant dynamic, we adopt POD method, the most efficient way of data compression.

Although POD has been used extensively in determining reduced order models of flow systems, relatively few attempts have been made to design active control strategies based on these models Ravindran [29]; Graham et al. [14],[15]; Atwell and King [5],; Arian et al. [3]. In Ravindran [29], Ravindran applied optimal control strategy to the reduced order model obtained from the finite element simulation of

a backward facing step flow. Graham et al. applied a similar technique to develop a reduced order model for cylinder wake, and used it to reduce the unsteadiness of the wake flow in Graham et al. [15]. Guaranteeing the stability of such a procedure which involves both reduced-order modelling and feedback control is not trivial, and as shown in Graham et al. [14], can lead to instability. In Atwell and King [5], Atwell and King overcame this problem by using a controller gain as a spatial snapshot to generate POD basis functions instead of using time snap shots. With such an approach, a satisfactory closed-loop performance was obtained but the number of basis functions required was larger. Arian et al. in Arian et al. [3] established convergence of the POD-based reduced-order technique in the presence of control input, by embedding it in a Trust-Region (TR), which resulted in the algorithm from exceeding a certain step size during each iteration. In this paper, our goal is to use the POD method to extract information about the mode shapes using the pressure measurements p in order to determine the control input u.

3.1 The POD method in flow field

POD method is nothing but a data compressing tool like Fourier series expansion. On confronting the POD method in control problem, one can ask the following question "Is there any relationship between the data compressing method and control strategy?" At the first glance, the data compressing tool seems to have nothing to do with control part. In fact, the POD method is not directly related to the control technique but plays an important role especially for simplifying the model.

The difficulty of the modelling was mentioned earlier. It seems almost impossible to make a fairly reliable model of impingement tone system because of incompressibility and sensitivity to the boundary condition etc. Even if the modelling of the system is completed, another difficulty still remains for the complexity of the system. Sometimes the model is mathematically too complicated to be controlled in online condition. Here POD method acts as a very useful tool for reducing the system's order not hurting the its principle dynamics because the model is reduced to a simple

form by projecting the governing equation on the dominant POD mode. The typical POD mode captures the system dynamics optimally for a given number of modes that the POD method is preferred.

With the goal of identifying a control input that has a maximum impact on the impingement tones even with small and slow change, we take a closer look at the feedback mechanism that produces the self-sustained oscillations of the impinging shear layer. Instability waves are generated by the acoustic excitation of the shear layer near the nozzle exit, which then convect down and evolve into spatially coherent structures. These waves in turn excite the shear layer at the nozzle exit, thereby providing the feedback. As indicated by the active control results in Fig.B-9, B-10, the introduction of the microjets at the nozzle has a large impact on the flow field even for a mass-flux addition of 0.5% of the main flow. Given the strong sensitivity of the flow-field as well as the tendencies of specific shear-layer modes to be driven into resonance to the boundary conditions at the nozzle, we chose the microjet pressure distribution at the nozzle exit as the control input. As stated in earlier chapter 2.1.4, a reduced-order model of the impingement tones based on the pressure data both without and with microjets at the nozzle can be derived as

$$\dot{x} = A(u)x \tag{3.1}$$

$$p = Cx \tag{3.2}$$

where x corresponds to the amplitudes of the impingement tones, p corresponds to the pressure measurements at the nozzle and u corresponds to the microjet pressure distribution along the nozzle.

3.2 The Control Strategy

At the earlier chapter, flow at the outer area of the nozzle are expressed by

$$p_+(r,\theta,z,t) = \sum_{i=1}^{L} X_i(t)\Phi_i(r,\theta,z) \tag{3.3}$$

where $X_i(t)$ is the state variable and $\{\Phi_i\}$ is a set of orthonormal functions satisfying the imposed boundary conditions viewed as the first L modes of the system. In order

to get the POD modes of the system, it is needed to calculate pressure at all flow points in three dimensional coordinate. This is not feasible either experimentally or computationally due to obvious constrains. However, our main goal is to model the impingement tones and it is worth noting that the key ingredients that contribute to their formation such as the initiation of the shear layer instability waves and their interaction with the acoustic waves appear to be localized at the jet nozzle. Therefore we derive the impingement tones model by focusing only on the POD of the pressure field close to the nozzle. That is, we derive the control strategy using the expansion:

$$p_+(r = R_j, \theta, z = z_{nozzle}, t) \equiv p(\theta, t) = \sum_{i=1}^{l} T_i(t)\phi_i(\theta) \tag{3.4}$$

where R_j is the radial position of the sensors on the lift plate. Note that ϕ_i's in equation (3.4) are, quite likely, a subset of Φ_i's in equation (2.32) which are the modes of the entire flow field. The state space equation corresponding to these reduced set of modes are given by:

$$\ddot{T}_j(t) = a_\infty^2 \sum_{i=1}^{l} (\nabla^2 \phi_i, \phi_j) T_i(t) \qquad j = 1, \cdots, l \tag{3.5}$$

with the inner product suitably defined. In vector form, this becomes:

$$\dot{T}(t) = \breve{A}(p_\mu) T(t). \tag{3.6}$$

The aim is to choose p_μ, the microjet pressure distribution such that $\|p_+(r, \theta, z, t)\|^2$ is minimized by making use of the pressure measurements made from the sensors placed on the upstream lift plate. In order to extract maximum possible information about the system, we adopt the Proper Orthogonal Decomposition(POD) Method.

If $F(x, t)$ is a generalized zero-mean flow variable, then the POD method seeks to generate an approximation for F by using separation of variable as

$$\hat{F}(x, t) = \sum_{i=1}^{l} T_i(t)\phi_i(x) \tag{3.7}$$

where $T_i(t)$ is the i^{th} spatial mode, l is the number of modes chosen, and t and x are the temporal and spatial variables respectively. The POD method consists of finding

ϕ_i such that the error $F(x,t) - \hat{F}(x,t)$ is minimized. This optimization problem can be stated as follows.

Denote $\{\phi_i(x)\}_{x=x_1,...,x_n} = \bar{\phi}_i \in \Re^n$. The POD method is the following optimization problem:

$$\min_{\Psi} J_m(\bar{\phi}_1, ..., \bar{\phi}_l) = \sum_{j=1}^{m} \|Y_j - \sum_{k=1}^{l} (Y_j^T \bar{\phi}_k)\bar{\phi}_k\|^2 \tag{3.8}$$

subject to :

$$\bar{\phi}_i^T \bar{\phi}_j = \delta_{ij},\ 1 \leq i,j \leq l, \Psi = [\bar{\phi}_1, ..., \bar{\phi}_l] \tag{3.9}$$

where $Y_j \in \Psi^n$ is the vector of flow data F at time $t = t_j$. By definition (3.8), Ψ is a POD modal set if it is a solution to the optimization problem (3.8) for any value of $l < m$. The POD modal set can be obtained using the "method of snapshots" mentioned from the equation (2.67) in earlier chapter.

Once the mode shapes are determined, we simply choose the control strategy as:

$$p_\mu(\theta) = k\phi_1(\theta) \tag{3.10}$$

where ϕ_1 is the most energetic mode in equation (3.4) and k is a calibration gain.

The complete closed-loop procedure therefore consists of collecting pressure measurements $p(\theta,t)$, expanding them using POD modes, determining the dominant mode ϕ_1, and matching the control input-which is the microjet pressure distribution along the nozzle-to this dominant mode as in equation (3.10).

The closed-loop control approach used here is distinctly different from the traditional feedback control paradigm where the control input is typically required to be modulated at the natural frequencies of the system. The latter, in turn, mandates that the external actuator has the necessary bandwidth for operating at the natural frequencies. In the problem under consideration, the edge tones associated with the flow-field are typically a few kilohertz. Given the current valve technology, modulating the microjets at the system frequencies is a near impossibility. The approach presented above overcomes this hurdle by modulating the control input, p_μ, at a slow time-scale, so that it behaves like a parameter. If this control input is chosen ju-

diciously, then even small and slow changes in this "parameter" can lead to large changes in the process dynamics.

3.3 The Experimental Support

3.3.1 The Experimental Setup

The Experimental Setup in Florida State University

The experiments were carried out to study jet-induced phenomenon on STOVL aircraft hovering in and out of ground effect using the STOVL supersonic jet facility of the Fluid Mechanics Research Laboratory (FMRL) located at the Florida State University. A schematic of the test geometry with a single impinging jet is shown in Fig.B-4

Fig.B-3 and Fig.B-4 show respectively the picture of the STOVL supersonic jet facility and its corresponding schematic of the experimental setup. The whole experimental setup is composed of three parts: structure mimicking aircraft body (lift plate and ground plane), measuring devices and compressor which makes the main jet possible to run on desired condition.

A circular plate of diameter D (25.4 cm $\sim$ 10d) was flush mounted with the nozzle exit. The circular plate, henceforth referred to as the 'lift plate', represents a generic aircraft planform. Through its concentric hole with exactly the same diameter as the nozzle exit, jet is issued. A 1 m $\times$ 1 m $\times$ 25 mm aluminum plate serves as the ground plane and is mounted directly under the nozzle on a hydraulic lift. Moving the ground plane to desired place, the hovering instance of the STOVL aircraft is realized. To simulate the hovering mode perfectly, the experiment should be conducted under the ground plane's moving condition. But we are focusing on an experiment conducted under the fixed height condition for the time being because this is the first step of series researches which ultimate goal is to reduce noise during taking off the ground. Moreover we didn't have enough knowledge about the flow property even for the fixed

heights condition. Even though it can travel from bottom to near the nozzle exit, almost every experiments are conducted between $h/d = 2 \sim 9$ where the barrier effect shows distinctly. Center of the plate is made up of glass to reveal the cross section of the flow. Here, PIV technique is used to investigate this cross section of the flow. The detailed explanation about PIV measurements will be covered later part of this section.

Flow control was implemented using sixteen microjets, mounted circumferentially around the main jet. Different from the conventional active noise control actuator like a speaker, the microjets contribute indirectly to noise reduction by changing the boundary condition of the main flow. At the first glance, it seems to respond somewhat late because extra steps are needed for changing boundary conditions to propagate the whole area. But its effect appears fast enough and the amount of noise reduction is much greater than other method. So far, the control was passive way flushing 16 microjets with 100 psi chamber pressure without considering varying experimental situation such as height change so that the effect was very limited to a certain condition. In this thesis, mode-matched control, an active control based on POD analysis is conducted and its effect will be compared to the passive control way to see how much gain improved from this new control strategy.

The microjet, an active actuator, is a small hole fabricated using 400 μm diameter stainless tubes and oriented at approximately 20° with respect to the main jet axis. The supply for the microjets was provided from compressed Nitrogen cylinder through a main and four secondary plenum chambers. Before reaching to each chamber, pressure passing thorough the pipe is controlled by electro-pneumatic servo valve, REXROTH. By adding a closed-loop PID control to this valve, the supply pressure is maintained to a desired value in spite of external disturbance and pressure drop during the experiment. Pressure signals of secondary plenum chamber are feeded into data acquisition board and compared to the target pressure. The difference are modified by PID gain and feeded into valve input signal again, which completed microjet PID control loop. All these process are managed by $LabVIEW^{TM}$ software installed in personal computer. The signal of the plenum pressure is initially captured by pres-

sure transducer, Scani Valve, and relayed into National Instrument AT0-M10-16E-2 data acquisition board but the target signal goes from an analog signal generator, PCI-6703, which occupies another slot in PC. Following the above logic, the supply pressures to each bank of microjets could be independently controlled and their intensities are kept constant regardless of external disturbance. The Microjets were operated over a range of NPR = 5 to 7 where the combined mass flow rate from all the microjets was less than 0.5% of the primary jet mass flux.

The unsteady loads generated by the impinging jet flow were measured using $Kulite^{TM}$ transducers on the lift plate and the ground plate. In addition, near-field noise was measured using a 0.635 cm $B\&K^{TM}$ microphones placed approximately 25 cm away from the jet oriented 90° to the jet axis. Six high frequency response miniature $Kulite^{TM}$ pressure transducers placed symmetrically around the nozzle periphery plate, at r/d =1.3 from the nozzle centerline, were used to obtain this distribution (Fig. B-5). The transducer outputs were conditioned and simultaneously sampled using National Instruments digital data acquisition cards and $LabVIEW^{TM}$ software. Standard statistical analysis techniques were used to obtain the spectral content and the Overall Sound Pressure Level (OASPL) from these measurements.

The nozzle is convergent-divergent (C-D) type with a design Mach number of 1.5. Air goes from a high-pressure blow-down compressed air facility to the nozzle. The facility is driven by a high-displacement reciprocating air compressor, can supply air at a maximum storage pressure 160 bars. Large storage tanks provide a total capacity of 10 m^3 and are capable of driving the Mach 1.5 jet continuously up to 40 min.

The throat and exit diameters (d, de) of the nozzle are 2.54cm and 2.75cm (see Fig.B-5 & B-4). The divergent part of the nozzle is a straight-walled conic section with 3° divergence angle from the throat to the nozzle exit. Although tests were conducted over a range of Nozzle Pressure Ratios (NPR, the ratio stagnation pressure to ambient pressure), the results discussed in the present paper are limited to NPR = 3.7. This specific ration corresponds to an ideally expanded Mach 1.5 jet velocity. For cross-sectional flow visualization, the jet was seeded with small ($\sim$1 μm in diameter) oil droplets generated using a modified Laskin nozzle and, investigating the large-

scale vortical structure, the ambient air was also seeded with smoke particle (5 μm in diameter) produced by a $Rosco^{TM}$ fog generator.

As mentioned before, the flow field was visualized using Particle Image Velocimeter (PIV) technique. This apparatus plays an important role in analysis on the flow field. Its main feature is to record two consecutive images in quick succession. From a series of two images, the velocity field is derived using a cross-correlation algorithm. The image is the oil or smoke particles illuminated by a double pulsed digitally sequenced Nd:YAG laser (Spectra-Physics, 400 mJ) which is a light sheet about 1.5 mm thickness created by suitable combination of spherical cylindrical lenses. The laser sheet position z with respect to the nozzle exit was varied from 1 d to 3 d to take a interested flow section. A schematic of the experimental arrangement of the PIV system is shown in Fig.B-8.

The images were recorded by a cross correlation CCD camera (Kodak ES 1.0). Its resolution is 1 k $\times$ 1 k and is operated in double pulsed mode. In this mode of operation, with proper synchronization with laser pulses, the camera can acquire double images at a rate of 15 images pairs per second. The present measurements were confined around 60 x 60 mm square cross section to ensure better image and to process it quickly. The time between pulses was optimized at 1.2 μs. The double pulsed images were acquired through an Imaging Technologies ICPCI board, which resides on a single slot of the PCI bus of a personal computer. An image matching approach was used for the digital processing of the image pairs to produce the displacement field. To achieve velocity data with high spatial resolution, a novel processing scheme was used, which are described in Lourenco, et.al. [21]. The marked advantage of this approach is that the velocity field is described at any point with second-order accuracy and thus computation of derivatives is accomplished with higher precision. At PIV measurement, the jet stagnation temperature was maintained at 320K. We slightly heated the jet nozzle to avoid the condensation happening on the glass when the gap between nozzle to ground is close enough. For further technology about the PIV, the reader can refer to a reference by A.Krothapalli et al. [19].

3.3.2 The Previous Study

Many trials to suppress the impingement tone using microjet have already been conducted by Florida State University members using the above experimental set up. Krothapalli [19] had exploited various phenomena of supersonic impingement flow using PIV. Followed by him, Shih et al. [35] used microjet to reduce impingement tones and found several factors affecting the level of noise generation and pressure fluctuation of the lift plate. The past research was rather proof-of-concept study to examine whether the microjet is a possible candidate to alleviate the adverse effect of supersonic impingement flow.

Shih [35]'s experiment indicates the possibility of microjet as a good actuator for suppressing noise. Supersonic impinging jets produce a very unsteady flow field, with high noise levels and discrete frequency acoustic tones. The instantaneous shadowgraph in Fig.B-9a show the a representative image for an uncontrolled - microjet off - impinging jet. We can see the distinct wave propagating up to the nozzle exit and bounded wave from the lift plate. A large-scale structure are also conspicuous near the ground plane. It is thought to be the main culprit for the flow entrainment and consequent cause of a large amount of lift loss suffered by STOVL aircraft during the hovering mode.

On the other hand, the effect of microjet is visible from the shadowgraph image in Fig.B-9b. The image is completely changed from the uncontrolled one in some features that totally different dynamics seem to be dominant at the controlled case. The ambient air becomes free from the acoustic wave and a distinct large-scale structure in the middle of the jet disappeared. In addition, an unexpected streak happens parallel to the main jet flow. It is worth noting that such streaks have been taken as an indicator of the presence of streamwise vorticity expected to be responsible for the improvement of performance.

PIV image in Fig.B-12 together with Planer Laser Scattering (PLS) in Fig.B-11 supports the role of the streamwise vorticity in noise reduction mechanism. Shih showed Fig.B-11, strongly indented shear layer images, in his paper [35]. Prompted by

the visual evidence, we quantitatively examined flow field using PIV at the previous research [20]. In the cross sectional image of main nozzle, 16 pairs of streamwise and counter streamwise vortices could be detected exactly where microjets were placed.

Fig.B-13 shows the narrowband spectra of the unsteady pressure signal on the lift plate for NPR = 3.7, h/d = 4.0. The presence on multiple tones is apparent by the discrete peaks in the spectra. By activating the microjet, distinct peaks are significantly diminished or entirely eliminated. Along with the narrow band noise reduction, the broadband noise amplitude was diminished to a certain extent. Such overall amplitude reduction patterns are seen in other data captured on the ground plane and near-field acoustic measurement collected by microphone (Alvi et al. [1]).

As can be seen in Fig.B-10, unsteady fluctuation at the lift plate is drastically reduced by introduction of microjet. These reduction can be found under ideally expanded nozzle condition (NPR = 3.7) as well as under-expanded case (NPR = 5.0). Inferring from the mechanism of impingement tone, the microjets is thought to disrupt the feedback loop, thereby prevent initiation of large scale structure and finally reduce the pressure fluctuation on the lift plate and noise generation over the ambient medium. The previous research [20] suggested a possible role of streamwise vorticity in this noise reduction mechanism. We believed that the streamwise vortices formed by microjet extract energy from spanwise vorticity and weaken the large scale structure. Consequently, the weakening vortical structure produces weaker acoustic waves when it impinges on the ground and attenuates the feedback loop.

Fig.B-10 are the overall reduction in the unsteady pressure and acoustic levels(P_{rms}) on the lift plate, ground plane and the near field noise for NPR=3.7 and 5. From the graph, we can easily notice that the microjet did reduce the overall sound pressure level to a certain degree under any circumstance, which is supported by three data set measured from different sensor positions. Another clear trend is that the amount of reduction is much larger for the under-expanded impinging jet, operated at NPR = 5 compared to the ideally expanded case.

The most noteworthy fact is the reduction is non-uniform with respect to the height (in Fig.B-10) and is unpredictable (as seen in Fig.B-14). It is well-known

that the properties of feedback loop of the uncontrolled jet, such as the amplitude and frequency of the impingement tones and the dominant instability modes in the flow, are highly sensitive to operating conditions. It is also worth noting due to the sensitivity of the feedback loop on the exact operating conditions, the effect of microjet control can vary even if the conditions are kept constant. As an example, although the height at which the microjets are minimally effective is h/d = 4.5 for the conditions in Fig.[B-14], it can on occasion shift to h/d = 4 or 5 during a particular test. Hence, an efficient control scheme should be able to adapt to the changes in the local flow conditions, on-line to provide optimal control over the entire operating range. The closed-loop control method mentioned in this thesis uses on-line measurements and active-adaptive algorithm to obtain a uniform and guaranteed reduction over a range of operating conditions in a reliable manner.

3.3.3 Result and Possible Mechanism of Microjet Effect

The mode-matched control strategy described above was implemented in the experimental apparatus described earlier, for a range of heights. At each height, in addition to the mode-matched control, the active control strategy as in Shih et al. [35] was also implemented. Since in the latter case, the spatial distribution of microjet pressure around the nozzle exit was kept uniform, it is referred to as "symmetric control." Since the latter does not use any system measurements and is determined a priori, the symmetric control can also be viewed as an open-loop control procedure. In order to ensure a fair comparison between the two control methods, the main nozzle was forced to operate under the constant condition throughout whole process.

The calibration constant k in equation (3.10) was chosen such that the minimum and maximum values of the POD mode over θ corresponds to 70psi and 120psi, respectively. These values were chosen since they ensured maximum effectiveness. Since the actuator configuration was such that it consisted of four microjet-banks that can be controlled independently and each bank in turn controlled four microjets, the bank input pressure was chosen as the average pressure values of the position where the four microjets are located. Fig.B-20 shows the shape of the first mode

and the suggested microjet bank pressure distribution for several heights. As can be seen in Fig.B-21, the mode-matched control strategy showed better performance at the experiment throughout all operational conditions, with a large improvement at heights h/d = 4, 4.5 and 5. The reason for this increased pressure reduction can be attributed to the percentage of energy contained in the dominant mode, which is used in the control strategy. As shown in table A.1, at heights 4 to 5, the energy content of the first mode is above 86% whereas at heights 2 and 3, the energy level drops to 55 % and below. As a result, the corresponding improvement in the mode-matched strategy also drops to about half the dB-value at heights 2 and 3 compared to at heights 4.0, 4.5, and 5.

The above result was very meaningful for the following reasons. First, the new control method caused a large amount of reduction as much as 9 dB at a certain height (h/d = 5.0) where the previous method couldn't generate any reduction in Fig.B-21. It means we now have possibility to realize even amount of noise reduction regardless of height distance. Second, new control method shows always better performance than the previous symmetric control strategy. To understand this phenomenon, we have to investigate the mechanism how the feedback loop of impingement tone system is intercepted and noise level is reduced by microjet action. Unfortunately, the mechanism is not well confirmed yet. As to the previous study, the streamwise vorticity is thought to extract the total kinetic energy from strong vorticity developed in azimuthal direction and weaken the development of large scale structure. As a result, the acoustic wave generated from impingement of the structure also becomes weak and finally the measured OASPL is reduced to some extent. While the microjet turns on, the intensity of the streamwise vorticity measured from PIV device is much higher than the amount can be generated from only 16 microjets' flushing. Recently, Shih et al. showed that a part of azimuthal, radial vorticity can be redirected to generate strong streamwise vorticity by the tilting and stretching of other vorticities in his paper [34]. The summary is as follows.

$$\frac{D\vec{\omega}}{Dt} = \vec{\omega} \cdot \nabla \vec{U} - \nabla \frac{1}{\rho} \times \nabla p + \nu \nabla^2 \vec{\omega} \tag{3.11}$$

where $\vec{\omega}$, $\vec{U}$, ρ, p, ν represent vorticity, velocity, density, pressure and kinematic viscosity, respectively. The above time-averaged vorticity transport equation shows how the streamwise vorticity is developed by other components. If both the baroclinic and the diffusion terms are neglected, the z directional streamwise vorticity transport equation can be expressed as follows.

$$\frac{D\omega_z}{Dt} = \omega_z \frac{\partial U_z}{\partial z} + \omega_r \frac{\partial U_z}{\partial r} + \omega_\theta (\frac{1}{r} \frac{\partial U_z}{\partial \theta}) \tag{3.12}$$

Directly, the streamwise voritcity (ω_z) is intensified by the tilting of the radial and azimuthal vorticity into the streamwise direction. The first term of the above equation represents the stretching of the existing streamwise vorticity. This term plays a crucial role only when the flow accelerates locally like under-expanded nozzle condition. Because we are considering only ideally expanded case at the experiment, this term is almost negligible. Clearly enough, the third term illustrates the tilting of azimuthal vorticity due to the streamwise velocity variation in θ direction. This mechanism is clearly understood, but it is not enough for explaining the whole source of streamwise vorticity.

$$\frac{D\omega_r}{Dt} = \omega_z \frac{\partial U_r}{\partial z} + \omega_r \frac{\partial U_r}{\partial r} + \omega_\theta (\frac{1}{r} \frac{\partial U_r}{\partial \theta}) \tag{3.13}$$

Following the above equation (3.13), we can find out the radial vorticity (ω_r) is developed by the tilting of azimuthal component described in the third term. As a result, the radial vorticity component is redirected into the streamwise vorticity. Affected by the increase of both ω_θ and ω_r, the streamwise vorticity is well developed finally. The detailed explanation for the streamwise vorticity generation mechanism can be referred to the Shih's paper [34].

At the mode-matched control strategy, the streawise velocity (U_z) and radial velocity (U_r) are set to be proportional to the first POD mode. Azimuthal variation of those velocities is thought to be systematically distributed so it can generate stronger streamwise vorticity than what the symmetric control strategy can generate. To verify this effect, detailed analysis based on the impingement tone model and support by PIV measurement should be conducted together. Furthermore, it is worthwhile to

find the optimal control strategy for the impingement tone system using the model. These directions will be pursued in the future.

Chapter 4

Summary and Concluding Remark

The objective of this research is to develop an active closed-loop control strategy to enhance STOVL aircraft performance. Most of adverse effects in STOVL aircraft system are caused by the feedback loop: the interaction between the ambient flow field and acoustic wave reflected from the ground plane. Previous investigators have found that the microjet injection into the main flow intercepted the interaction and generated a significant amount of noise reduction. In this thesis we explored a control strategy to reduce the noise more effectively than previous control method.

In the chapter 2, a mathematical model called "vortex-sheet model" was introduced and its validity was supported from two experimental observations. The staging phenomena of peak frequency predicted from the analytical model was also seen in experimental data and the amount of interval between one peak to next is observed to be decreased as the gap between the ground and the lift plate becomes farther. Even though the model is very close to the real system, it is too complicated to be used for a plant to be controlled in real-time. Hence, the Proper Orthogonal Decomposition, a tool for extracting the dominant dynamics from the experimental data was presented to reduce the complexity of the model.

In the chapter 3, a "mode-matched control" strategy based on the POD mode of the flow field was introduced. Its effectiveness was proven from the experimental data and one possible explanation how the microjet can cause the significant amount of noise reduction. For the experiment, we focused just on the ideally expanded

nozzle case. In fact, the best noise reduction by microjets happens when the nozzle is running in an under-expanded condition. As the nozzle goes from under-expanded to over-expanded condition, it becomes more difficult to control. Even thought the worst condition requiring noise reduction is over-expanded, because the OASPL of over-expanded case is usually less higher than ideally expanded nozzle and less prone to noise, it is more important in practice to find a control strategy for the ideally expanded condition. To compare its efficacy to the past open-loop control strategy, OASPL of two cases were compared under the same flow condition. The result showed that the amount of noise reduction by "mode-matched control" is much larger than that by "symmetric control" method. It is very promising in that we have possibility to cause even noise reduction regardless of height change and new method is better than open-loop control under any condition.

In further research, the optimal control strategy for the impingement tone system using the more model needs to be pursued and the mechanism about the noise reduction needs to be supported from various experimental investigations.

Appendix A

Tables

Table A.1: The energy content of the first four modes at each height (NPR=3.7)

h/d	Mode1	Mode2	Mode3	Mode4
2.0	0.4615	0.2488	0.1785	0.1111
3.0	0.5515	0.2745	0.1144	0.0597
4.0	0.8609	0.0691	0.0443	0.0257
4.5	0.8836	0.0517	0.0389	0.0258
5.0	0.8736	0.0757	0.0314	0.0194

Table A.2: Comparison of peak frequency interval (Hz) NPR=3.7, M =1.5

h/d	Experiment data	Model prediction	Percent of discrepancy
2.0	2688.67	2525.0	6.1
3.0	1926.88	2250.0	16.8
4.0	1473.20	1666.7	13.1
4.5	1289.01	1500.0	16.4
5.0	1137.50	1350.0	18.7
6.0	1196.25	1125.0	6.0

Appendix B

Figures

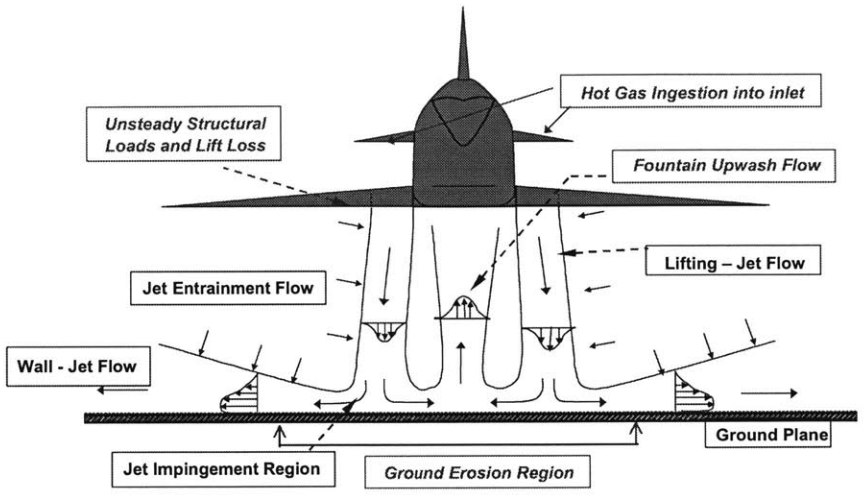

Figure B-1: Flow field created by the propulsion system around a STOVL aircraft

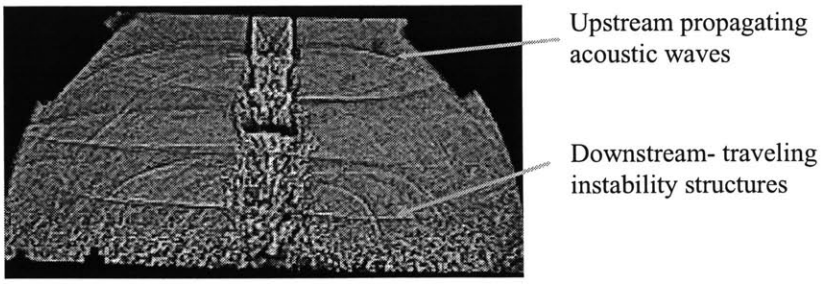

Figure B-2: Instantaneous shadowgraphs of a supersonic impinging jet at NPR = 3.7, $h/d = 5.5$

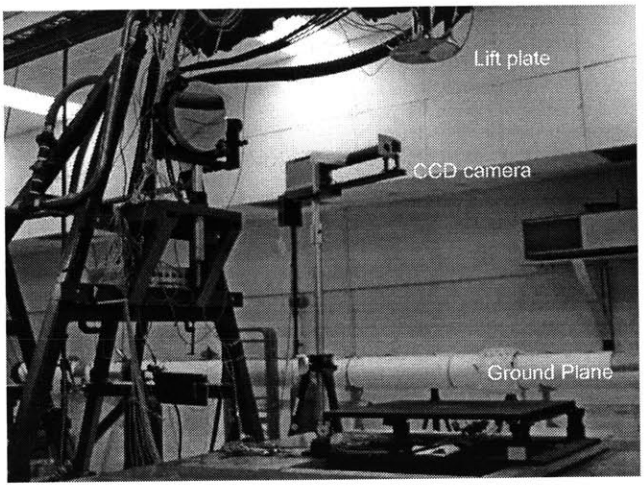

Figure B-3: The experimental set up of Fluid Mechanics Research Laboratory in Florida State University

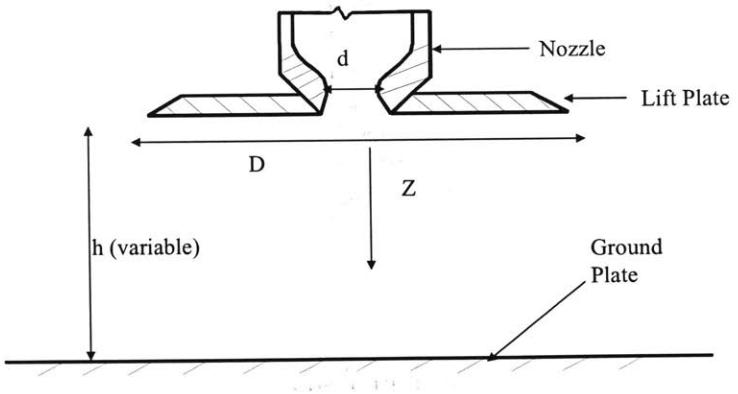

Figure B-4: Schematic of the experimental arrangement

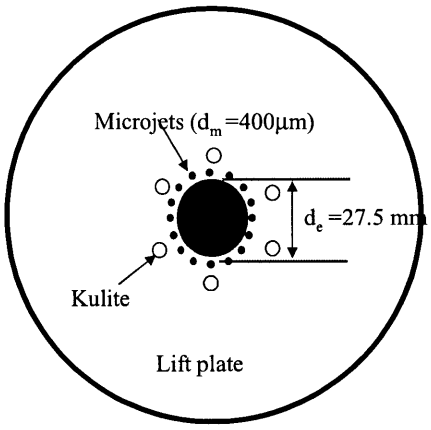

Figure B-5: Schematic of the lift plate

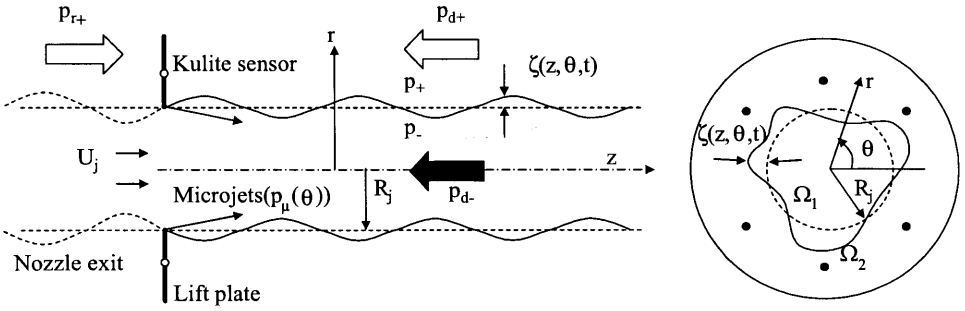

Figure B-6: Vortex-sheet model for impingement tones control problem

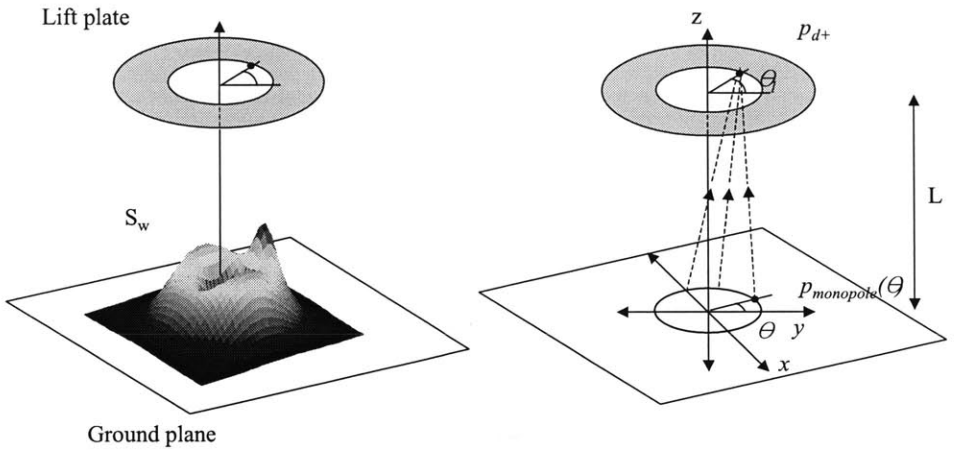

Figure B-7: Expected shear layer intensity distribution (a), coordinate system used for calculating acoustic excitation (b).

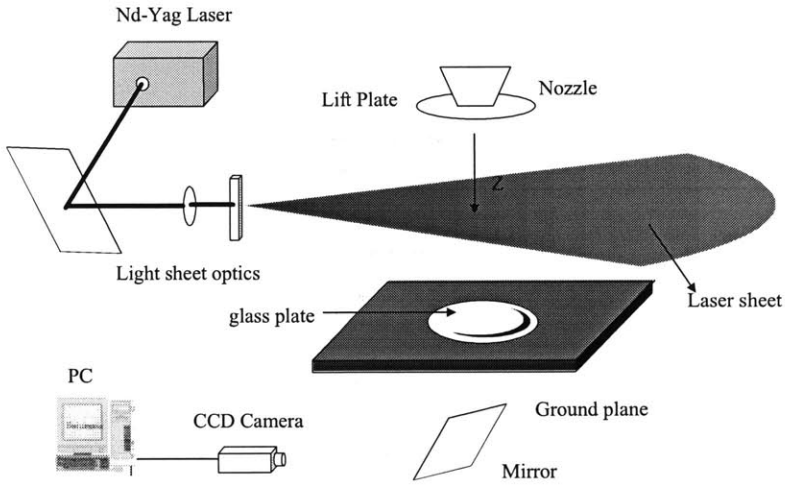

Figure B-8: Schematic diagram of PIV mearsuring process

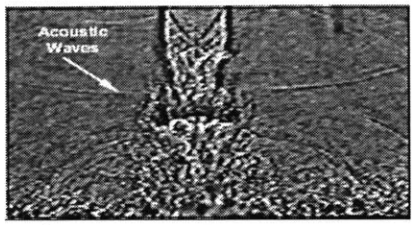

a)

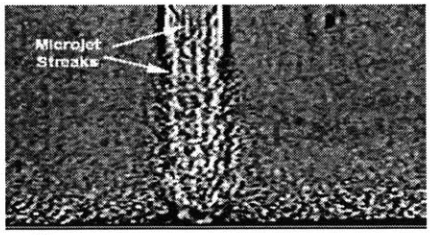

b)

Figure B-9: Instantaneous shadowgraph images of a supersonic impinging jets without (a) and with control (b) at NPR = 3.7, $h/d = 4$

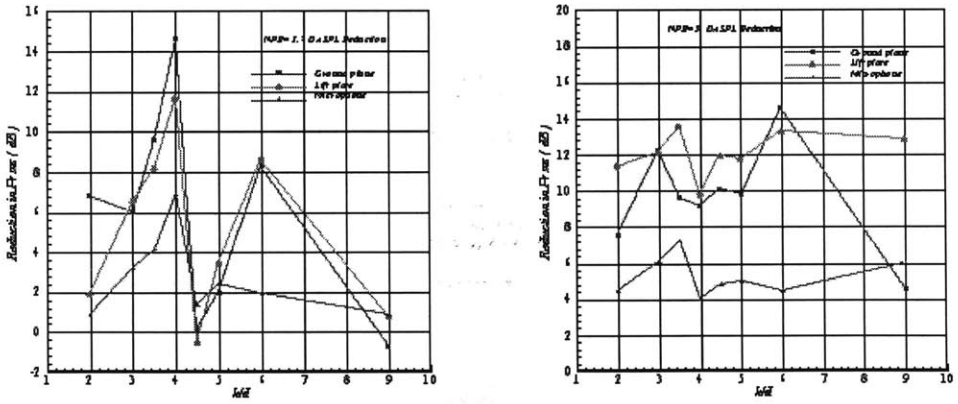

(a) (b)

Figure B-10: Reductions in fluctuating pressure intensities as a function of h/d, NPR = 5 (a) and NPR = 3.7 (b)

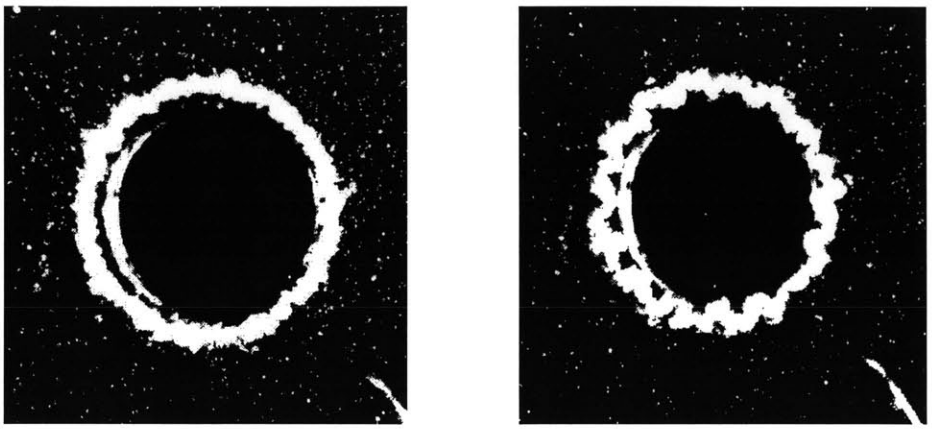

No Control With Control

(a) Instantaneous PLS images

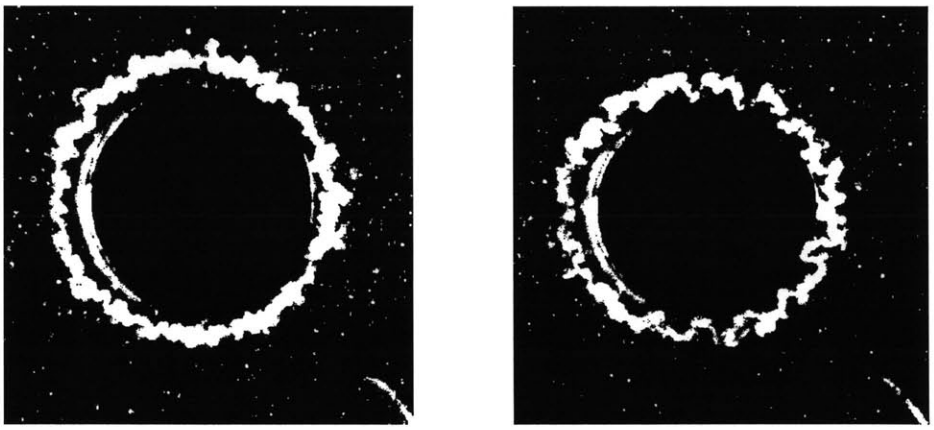

No Control With Control

(b) Time-averaged PLS images

Figure B-11: PLS images taken at one diameter downstream of nozzle, NPR = 5.0, $h/d = 4.0$; (a)Instantaneous image, (b)Time-averaged image

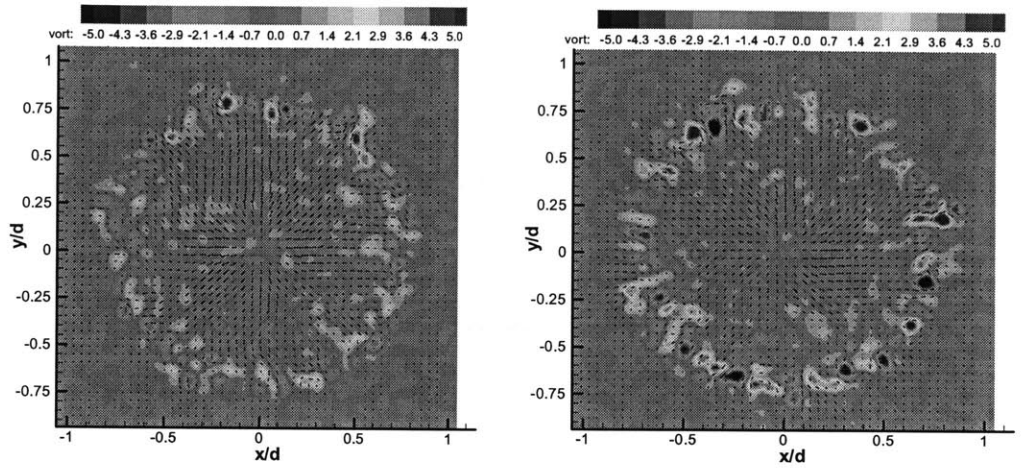

No Control With Control

(a) Instantaneous PIV images

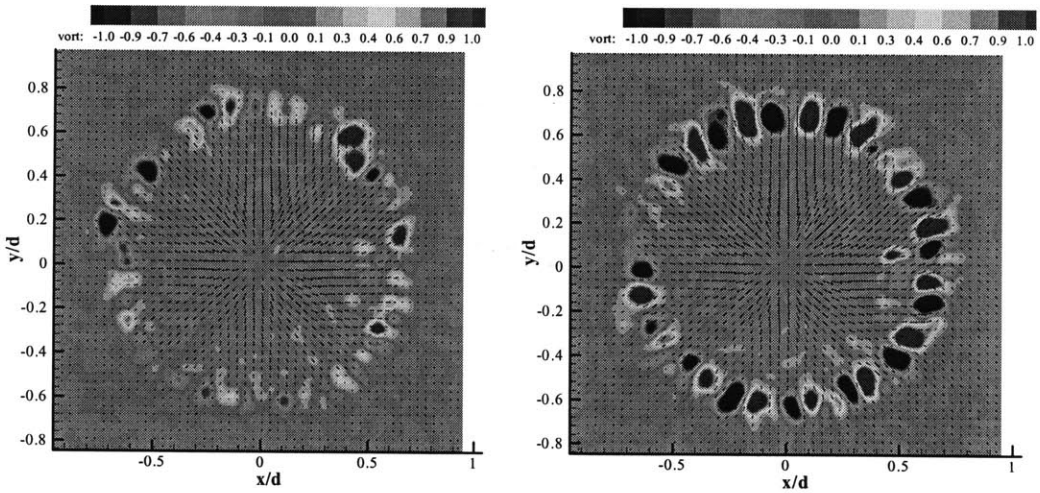

No Control With Control

(b) Time-averaged PIV images

Figure B-12: Streamwise vorticity distribution at the z/d = 1.0 cross plane of the jet flow NPR = 5.0, $h/d = 4.0$; (a)Instantaneous image, (b)Time-averaged image

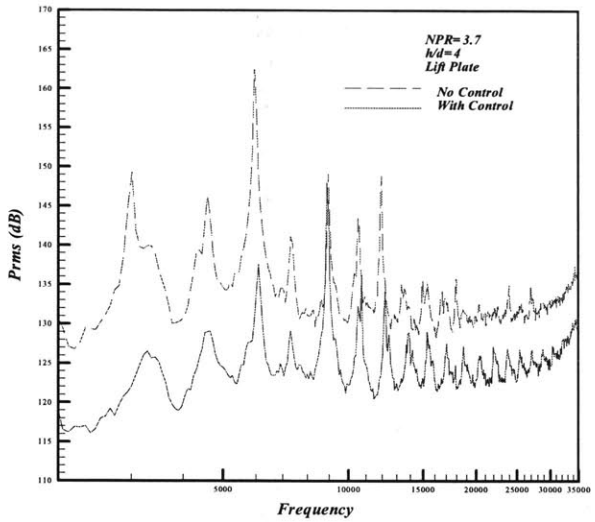

Figure B-13: Frequency spectra for unsteady pressure on the lift plate of NPR = 3.7, $h/d = 4.0$

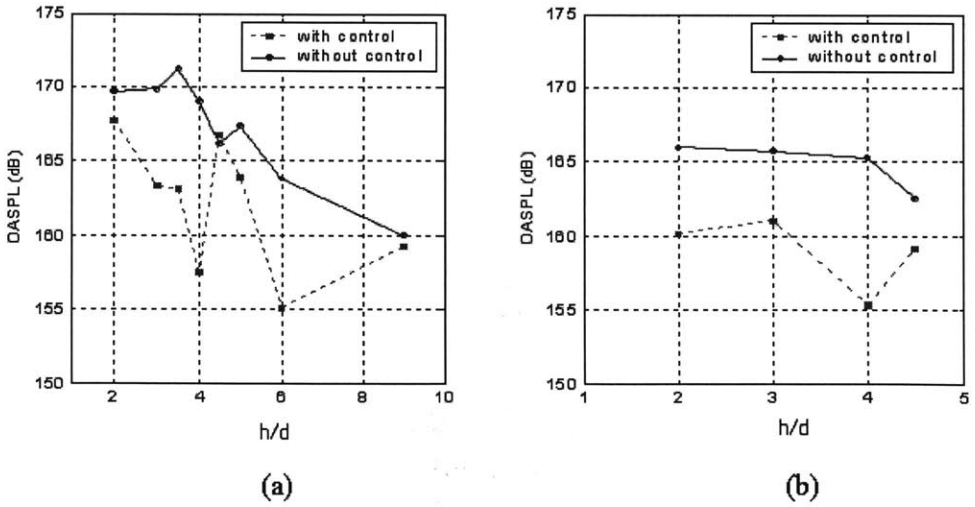

Figure B-14: Microjet effectiveness on different trials (NPR = 3.7) conducted on Sep. 2000 (a) and Dec. 2001 (b)

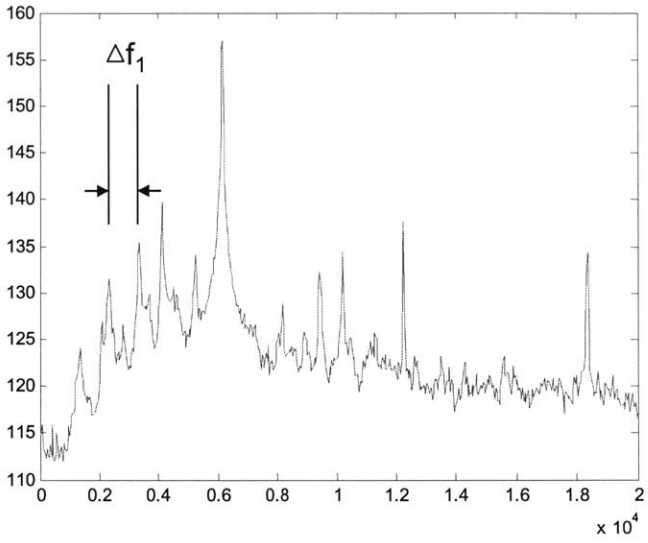

(a)

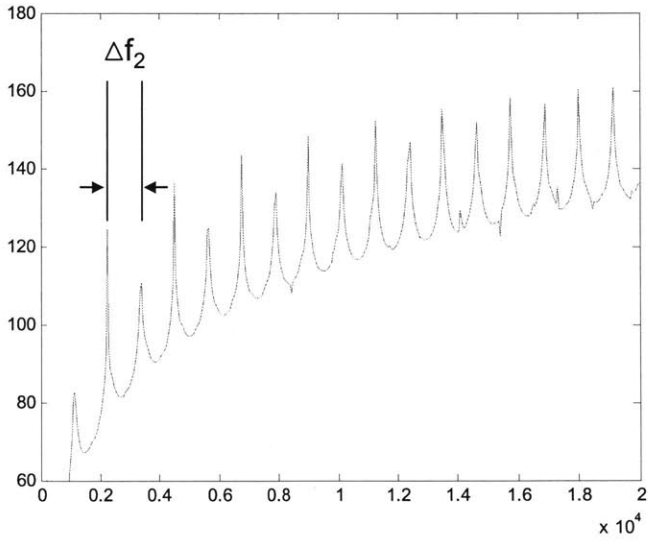

(b)

Figure B-15: Frequency spectra for unsteady pressure on the lift plate of NPR = 3.7, $h/d = 6.0$ (a) and model prediction of NPR = 6.0 (b)

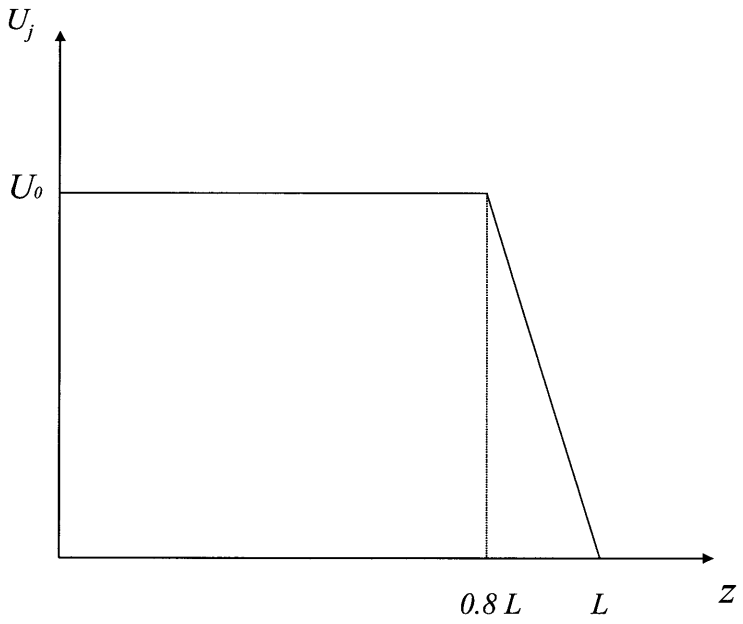

Figure B-16: The idealized centerline velocity

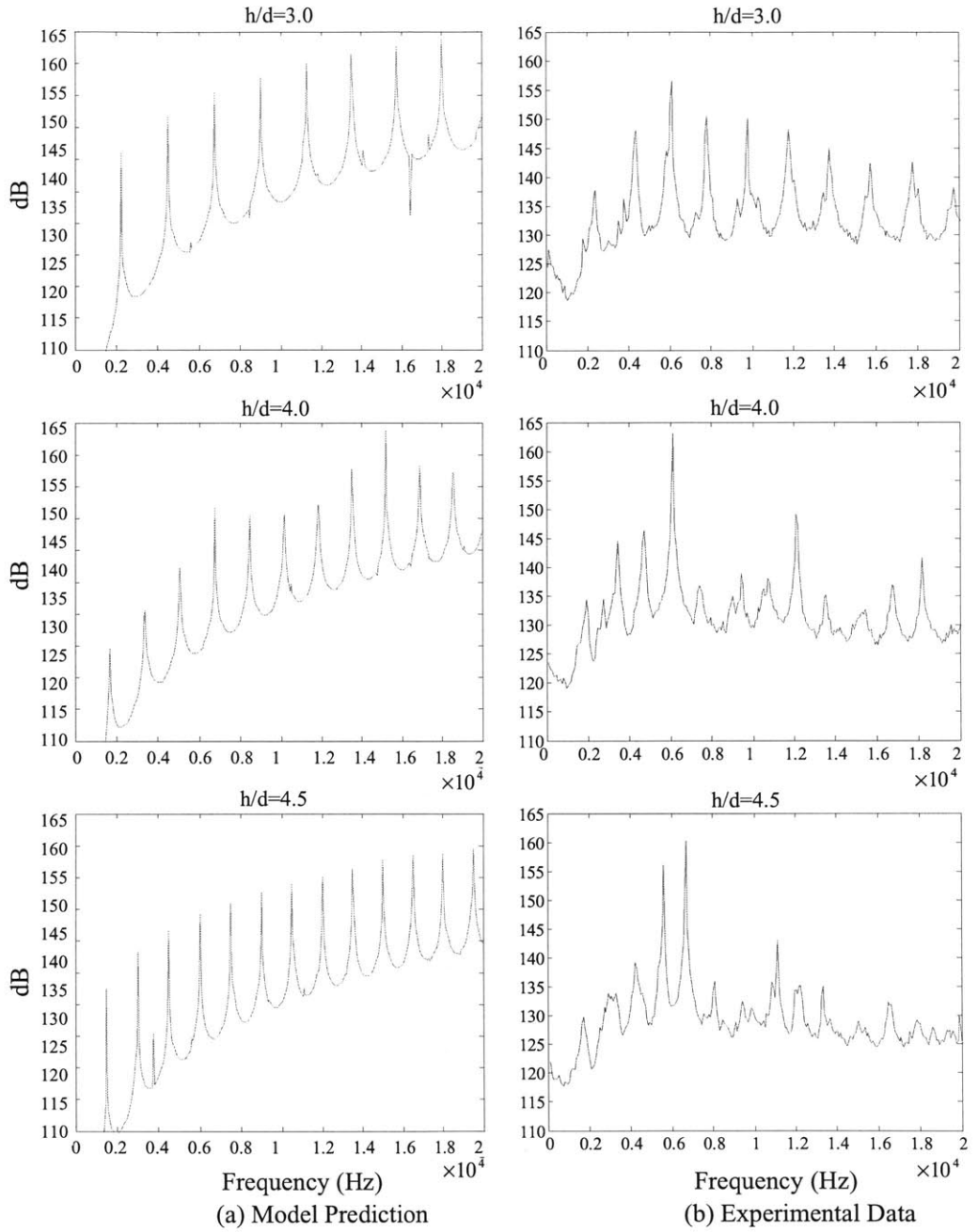

Figure B-17: Frequency spectra of the unsteady pressure on the lift plate at NPR = 3.7: (a) Experimental data, and (b) Model prediction. Note that the amplitude scales in (a) and (b) are different.

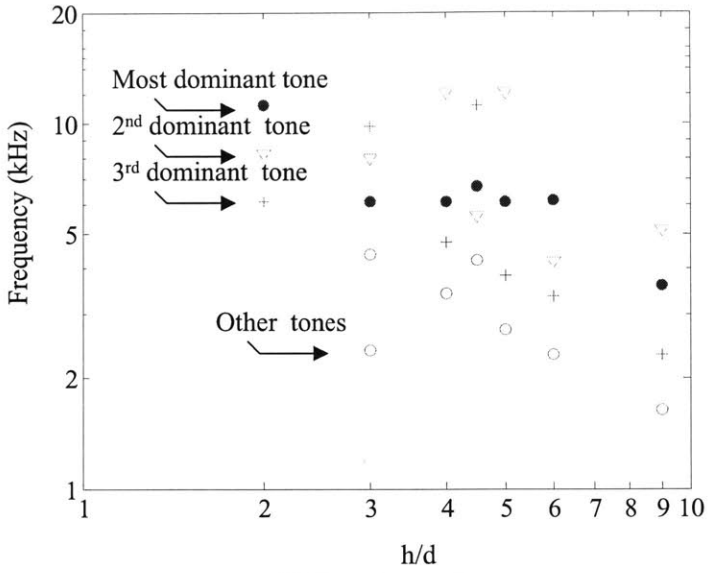

(a) Experimental Data

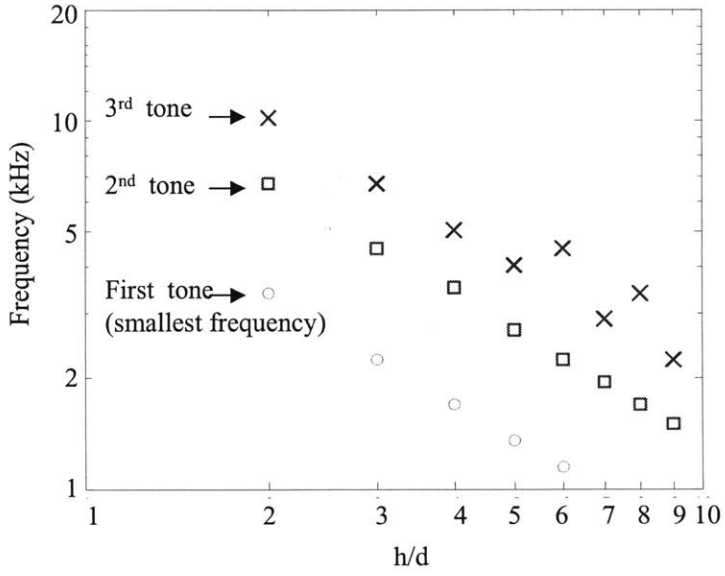

(b) Model Prediction

Figure B-18: Variation of frequency of three impinging tones with h/d at NPR = 3.7: (a) Experimental data, and (b) Model Prediction.

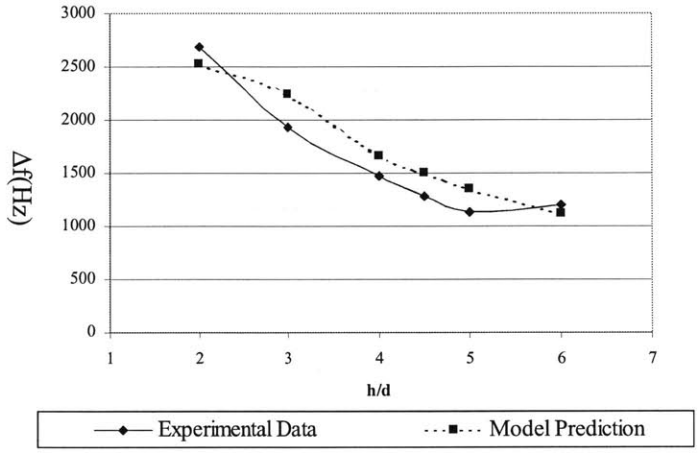

Figure B-19: Peak frequency interval of experimental data and model prediction (NPR=3.7, M = 1.5)

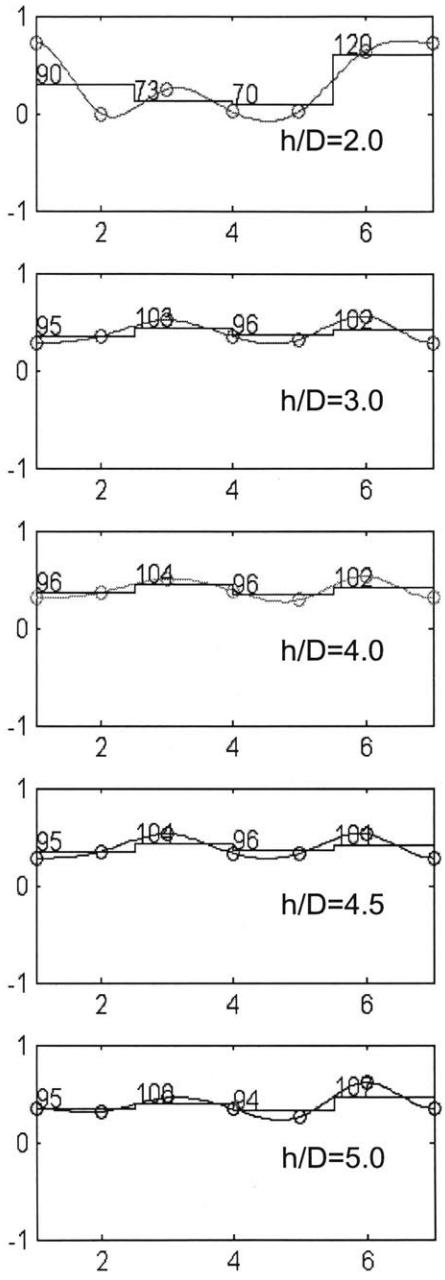

Figure B-20: The first mode shape and suggested pressure for each height. x axis is transducer position, y axis is normalized mode value

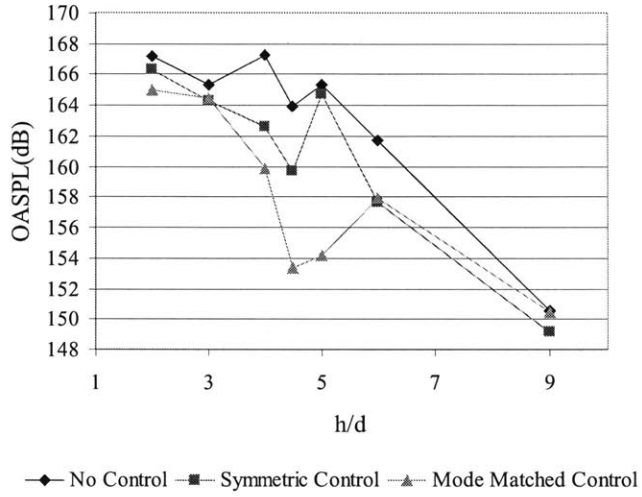

Figure B-21: Overall sound pressure levels(OASPL) for different control (NPR=3.7)

Bibliography

[1] F.S. Alvi, R. Elavarsan, C. Shih, G. Garg, and A. Krothapalli. Control of supersonic impinging jet flows using microjets. Technical Report 2000-2236, AIAA Paper, 2000.

[2] F.S. Alvi and K.G. Iyer. Mean and unsteady flowfield properties of supersonic impinging jets with lift plates. Technical Report 2000-25, NASA/CR-2000-210124,ICASE, 2000.

[3] E. Arian, M. Fahl, and E.W. Sachs. Trust-region proper orthogonal decomposition for flow control. Technical Report 99-1829, AIAA Paper, 1999.

[4] R.E.A. Arndt, D.F. Long, and M.N. Glauser. The proper orthogonal decomposition of pressure fluctuations surrounding a turbulent jet. *Journal of Fluid Mechanics*, 340:1–33, 1997.

[5] J.A. Atwell and B.B King. Proper orthogonal decomposition for reduced basis feedback controllers for parabolic equations. *Mathematical and Computer Modeling*, 33, 2001.

[6] P. Bakewell and J.L. Lumley. Viscous sublayer and adjacent wall region in turbulent channel pipe flow. *Physics of Fluids*, 10:1180–1189, 1967.

[7] G. Berkooz, P. Holmes, and J. L. Lumley. The proper orthogonal decomposition in the analysis of turbulent flows. *Annual Reviews of Fluid Mechanics*, 25:539–575, 1993.

[8] K.M. Cipolla, A. Liakopoulos, and D.O. Rockwell. Quantitative imaging in proper orthogonal decomposition of flow past a delta wing. *AIAA Journal*, 36:1247–1255, 1998.

[9] J.H. Citriniti and W.K. George. Reconstruction of the global velocity field in the axisymmetric mixing layer utilizing the proper orthogonal decomposition. *Journal of Fluid Mechanics*, 418:137–166, 2000.

[10] J. Delville, L. Ukeiley, L. Cordier, J.P. Bonnet, and M. Glauser. Examination of large-scale structures in a turbulent plane mixing layer. part. 1. proper orthogonal decomposition. *Journal of Fluid Mechanics*, 391:91–122, 1999.

[11] R. Elavarasan, A. Krothapalli, L. Venkatakrishnan, and L. Lourenco. Suppression of self-sustained oscillations in a supersonic impinging jet. *AIAA Journal*, 39(12), 2001.

[12] D.R. Glass. Effect of acoustic feedback on the spread and decay of supersonic jets. *AIAA Journal*, 6(6):1890–1897, 1968.

[13] P. Gottlieb. Sound source near a velocity discontinuity. *The Journal of the Acoustical Society of America*, 32(9), 1960.

[14] W.R. Graham, J.P. Peraire, and K.Y. Tang. Optimal control of shedding using low-order models; part i: Open-loop model development. *International Journal for Numerical Methods in Engineering*, 44, 1999.

[15] W.R. Graham, J.P. Peraire, and K.Y. Tang. Optimal control of shedding using low-order models; part ii: Model-based control. *International Journal for Numerical Methods in Engineering*, 44, 1999.

[16] C.M. Ho and N.S. Nosseir. Dynamics of an impinging jet. part 1. the feedback phenomenon. *Journal of Fluid Mechanics*, 105, 1981.

[17] P. Holmes, J.L. Lumley, and G. Berkooz. *Turbulence, coherent structures, dynamical systems and symmetry.* Cambridge University Press, 1996.

[18] P. Huerre and P.A. Monkewitz. Absolute and convective instabilities in free shear layers. *J. Fluid Mech.*, 159:151–168, 1985.

[19] A. Krothapalli, E. Rajakuperan, F.S. Alvi, and L. Lourenco. Flow field and noise characteristics of a supersonic impinging jet. *Journal of Fluid Mechanics*, 392:155–181, 1999.

[20] H. Lou, F.S. Alvi, C. Shih, J. Choi, and A. Annaswamy. Active control of supersonic impinging jets: Flowfield properties and closed-loop strategies. Technical Report 2002-2728, AIAA Paper, 2002.

[21] L.M. Lourenco and A. Krothapalli. Mesh-free second order accurate algorith for piv processing. Proc. Intl Conf. On Optical Technology and Image Processing in Fluid, Thermal and Combustion Flows, page 224, 1998.

[22] M. Ma, G.S. Karamanos, and G.E. Karniadakis. Dynamics and low-dimensionality of a turbulent near wake. *Journal of Fluid Mechanics*, 140:29–65, 2000.

[23] A. Michalke. Survey on jet instability theory. *Prog. Aerospace Science*, 21, 1984.

[24] G. Neuwerth. Acoustic feedback of a subsonic and supersonic free jet which impinges on an obstacle. Technical Report TTF-15719, NASA, 1974.

[25] A.J. Newman. Model reduction via the karhunen-loeve expansion part i: An exposition. Technical Report T.R. 96-32, Institute for System Research, University of Maryland, USA, 1996.

[26] L.J. Poldervaart, A.P.J. Wijnands, L.H.A.M vanMoll, and E.J. vanVoorthuisen. Modes of vibration. *J.Fluid Mech*, 78:859–862, 1976.

[27] A. Powell. On edge tones and associated phenomena. *Acoustica*, 3:233–243, 1953.

[28] A. Powell. The sound-producing oscillations of round underexpanded jets impinging on normal plates. *J. Acoust. Soc. Am*, 83(2):515–533, 1988.

[29] S. Ravindran. A reduced order approach to optimal control of fluids using proper orthogonal decomposition. *International Journal for Numerical Methods in Fluids*, 34:425–448, 2000.

[30] D. Rempfe. On the structure of dynamical systems describing the evolution of coherent structures in a convective boundary layer. *Physics of Fluids*, 6:1402–1404, 1994.

[31] C.W. Rowley, T. Colonius, and R.M. Murray. Pod based models of self-sustained oscillations in the flow past an open cavity. Technical Report 2000-1969, AIAA Paper, 2000.

[32] M. Sheplak and E.F. Spina. Control of high-speed impinging-jet resonance. *AIAA Journal*, 32(8):1583–1588, 1994.

[33] C. Shih, F.S. Alvi, and D. Washington. Effect of counterflow on the aeroacoustic properties of a supersonic jet. *AIAA Journal of Aircraft*, 36(2):451–457, 1999.

[34] C. Shih, H. Lou, F.S. Alvi, and A. Krothapalli. Microjet control of supersonic impinging jets - control strategy and physical mechanisms. Technical Report 2002-6009, AIAA Paper, 2002.

[35] C. Shih, H. Lou, G. Garg, and A. Krothapalli. Adaptive flow control of supersonic impinging jets. Technical Report 2001-3027, AIAA Paper, 2001.

[36] L. Sirovich. Turbulence and the dynamics of coherent structures; part 1: Coherent structures. *Quarterly Appl. Math.*, 45(3):561–571, October 1987.

[37] L. Sirovich. Turbulence and the dynamics of coherent structures; part 2: Symmetries and transformations. *Quarterly Appl. Math.*, 45(3):573–582, October 1987.

[38] L. Sirovich. Turbulence and the dynamics of coherent structures; part 3: Dynamics and scaling. *Quarterly Appl. Math.*, 45(3):583–590, October 1987.

[39] L. Sirovich and J.D. Rodriguez. Coherent structures and chaos: A model problem. *Physics Lett. A*, 120:211–214, 1987.

[40] C.K.W Tam and K.K. Ahuja. Theoretical model of discrete tone generation by impinging jet. *J. Fluid Mech*, 214:67–87, 1900.

[41] D. Tang, D. Kholodar, J. Juang, and E.H. Dowell. System identification and proper orthogonal decomposition method applied to unsteady aerodynamics. *AIAA Journal*, 39(8):1569–1576, 2001.

[42] Y. Umeda, H. Maeda, and L. Ishii. Discrete tones generated by the impingement of a high speed jet on a circular cylinder. *Physics of Fluids*, 30, 1987.

[43] S. Volkwein. Proper orthogonal decomposition and singlular value decomposition. Technical Report 153, SFB-Preprint, 1999.

[44] F.R. Wagner. The sound and flow field of an axially symmetric free jet upon impact on a wall. Technical Report F-13942, NASA TT, 1971.